Donor-Acceptor-Functionalized Tetraethynylethenes with Nitrothienyl Substituents: Structure-Property Relationships

by **Rik R. Tykwinski**[a]), **Anouk Hilger**[b]), **François Diederich***[c]), **Hans Peter Lüthi**[b])*, **Paul Seiler**[c]), **Volker Gramlich**[d]), **Jean-Paul Gisselbrecht**[e]), **Corinne Boudon**[e]), and **Maurice Gross**[e])

[a]) Department of Chemistry, University of Alberta, Edmonton, Alberta, T6G 2G2 Canada
[b]) Laboratorium für Physikalische Chemie, ETH-Zentrum, Universitätstrasse 22, CH-8092 Zürich
[c]) Laboratorium für Organische Chemie, Eidgenössische Technische Hochschule, ETH-Zentrum, Universitätstrasse 16, CH-8092 Zürich
[d]) Laboratorium für Kristallographie, Eidgenössische Technische Hochschule, ETH-Zentrum, Sonneggstrasse 5, CH-8092 Zürich
[e]) Laboratoire d'Electrochimie et de Chimie Physique du Corps Solide, U.M.R. au CNRS, no. 7512, Faculté de Chimie, Université Louis Pasteur, 1 et 4, rue Blaise Pascal, F-67008 Strasbourg Cedex

Dedicated to the memory of *Michael C. Zerner*

Tetraethynylethenes (TEEs) functionalized with donor (4-(dimethylamino)phenyl) and acceptor (5-nitro-2-thienyl) groups were prepared by Pd^0-catalyzed *Sonogashira* cross-coupling reactions (*Schemes 1–6*). The physical properties of these novel chromophores were examined and compared with those of analogous systems containing 4-nitrophenyl instead of 5-nitro-2-thienyl acceptor groups. X-Ray crystal-structure analyses showed the π-conjugated frameworks of **2**, **11**, and **13**, including the TEE core and all aryl moieties, to be nearly perfectly planar (*Figs. 1*, *3*, and *4*). In contrast, one 4-(dimethylamino)phenyl group in **10** is rotated almost 90° out of the molecular plane, presumably due to crystal-packing effects (*Fig. 2*). The analysis of bond lengths and bond angles revealed little, if any, evidence of intramolecular ground-state donor-acceptor interactions. The electrochemical behavior of nitrothienyl-substituted TEEs is similar to that of the corresponding nitrophenyl-functionalized derivatives (*Table 3*). The nitrothienyl groups were reduced at -1.23 V (*vs.* the ferrocene/ferricinium couple, Fc/Fc^+), regardless of the degree or pattern of other substitutions. For nonsymmetrical TEE **13**, the reduction of the nitrothienyl group at -1.23 V is followed by a reduction of the nitrophenyl group at -1.40 V, a potential typical for the reduction of other nitrophenyl-substituted TEEs, such as **17**–**20**. UV/VIS Spectroscopy showed a consistently lower-energy absorption cutoff for nitrothienyl derivatives compared with the analogous nitrophenyl-substituted TEEs that confirms a lowering of the HOMO-LUMO gap as a result of nitrothiophene substitution (*Figs. 5* and *6*). A comparison of the tetrakis-arylated TEEs **11**, **13**, and **20** clearly showed a steady bathochromic shift of the longest-wavelength absorption maximum and the end-absorption upon sequential replacement of nitrophenyl by nitrothienyl groups. Quantum-chemical computations were performed to explain a number of complex features of the electronic absorption spectra. All empirical features of relevance in the experimental UV/VIS spectra for **2**, **5**, **6**, and **17**–**19** were correctly reproduced by computation (*Tables 4* and *5*). The combination of theory and experiment was found to be very useful to explain the particular acceptor properties of the 5-nitro-2-thienyl group.

1. Introduction. – Conjugated organic compounds are expected to make significant contributions to materials science, since they combine interesting electronic and photonic properties with synthetic versatility, stability, and processability [1]. Importantly, they provide the flexibility for optimization – through synthesis – of desired properties by controlled manipulation of the molecular and electronic structure. A basic understanding of structure-property relationships is crucial for the rational development of useful organic materials. Such a comprehension is reached in

investigations of series of structurally related molecules with properties that can readily be tuned through functional-group manipulation.

Tetraethynylethene (TEE, 3,4-diethynylhex-3-ene-1,5-diyne; **1**) is an outstanding π-conjugated scaffold for appending electron-donating and/or -accepting substituents so that both structural and electronic effects on optoelectronic properties may be investigated [2–4]. In recent years, the effects of linear, cross, and two-dimensional (2-D) conjugation modes on physical properties of donor-acceptor(D-A)-substituted TEEs were comprehensively analyzed [5–9]. These studies revealed a profound influence of donor-acceptor (D-A) effects on structural [5][6], electrochemical [7], luminescent [5][6], and second and third-order nonlinear optical (NLO) [8–13] properties of these materials.

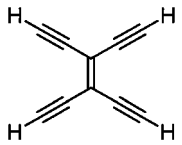

1

In continuation of our efforts to improve the NLO responses of D-A-functionalized TEEs, we substituted 4-nitrophenyl acceptors by 5-nitro-2-thienyl moieties. Benzenoid aromaticity is reduced in the thiophene ring, as compared to benzene, and this leads to an increased capacity to transmit linear π-electron conjugation and an enhanced nonlinear optical response. This has been demonstrated theoretically [14–17] and experimentally for both second- [18–25] and third-order [26–30] NLO effects. Our recent investigations with 2-(5-nitro-2-thienyl)-substituted D-A-functionalized TEEs confirmed that thiophene rings do indeed enhance third-order NLO effects, as measured by solution-state third-harmonic generation [11][13]. Here, we describe the synthesis of these compounds, as well as a detailed analysis of their structural and electronic properties by X-ray crystallography, electronic absorption spectroscopy, electrochemical analysis, and quantum-chemical calculations.

2. Results and Discussion. – 2.1. *Synthesis of 2-(5-Nitro-2-thienyl)-Substituted Tetraethynylethenes.* The synthesis of *trans*-D-A-substituted TEE **2** started with mono-donor-substituted **3** [5][6], which was deprotected to give the ethynyl derivative **4** (*Scheme 1*) [5][6]. Pd^0-Catalyzed *Sonogashira* cross-coupling [31] with 2-iodo-5-nitrothiophene [32] afforded **2** as a deep-red solid. Irradiation at λ 366 nm induced *trans* → *cis* isomerization [5][6][33] to yield a mixture of **2** and *cis*-isomer **5** in a ratio of *ca.* 1:2, which could be readily separated.

The geminally D-A-substituted TEE **6** was synthesized by stepwise cross-coupling starting from gem-dibromoethene **7** [34] (*Scheme 2*). Coupling with 4-ethynyl-*N*,*N*-dimethylaniline [35], then with (ethynyl)trimethylsilane gave TEE **8**. Removal of the Me_3Si group, followed by cross-coupling with 2-iodo-5-nitrothiophene, provided **6** as a light-red solid.

Scheme 1. *Synthesis of* trans- *and* cis-*Bis-Arylated TEEs* **2** *and* **5**

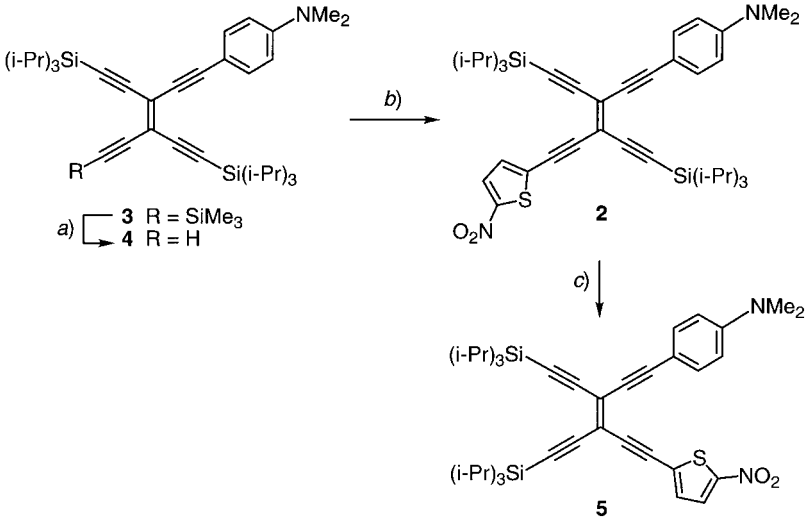

a) K_2CO_3, wet MeOH, THF, r.t., 2 h. *b*) 2-Iodo-5-nitrothiophene, $[PdCl_2(PPh_3)_2]$, CuI, Et_3N, r.t., 12 h; 62% (from **3**). *c*) *hν* ($\lambda = 366$ nm), hexane, r.t., 2 h; 67%.

Scheme 2. *Synthesis of Geminally Bis-Arylated TEE* **6**

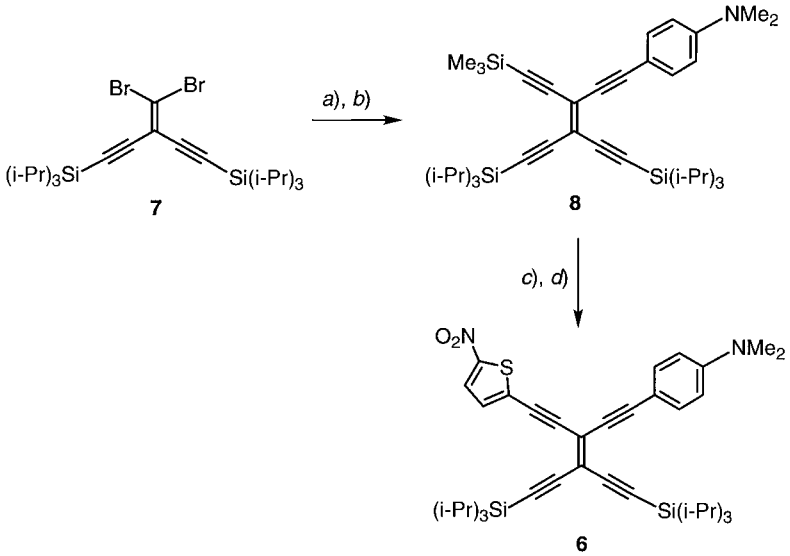

a) 4-Ethynyl-*N*,*N*-dimethylaniline, $[PdCl_2(PPh_3)_2]$, CuI, Et_3N, r.t., 24 h. *b*) (Ethynyl)trimethylsilane, r.t., 8 h; 19% (from **7**). *c*) K_2CO_3, wet MeOH, THF, r.t., 2 h. *d*) 2-Iodo-5-nitrothiophene, $[PdCl_2(PPh_3)_2]$, CuI, Et_3N, r.t., 12 h; 74% (from **8**).

Scheme 3. *Synthesis of Tris-Arylated TEE* **10**

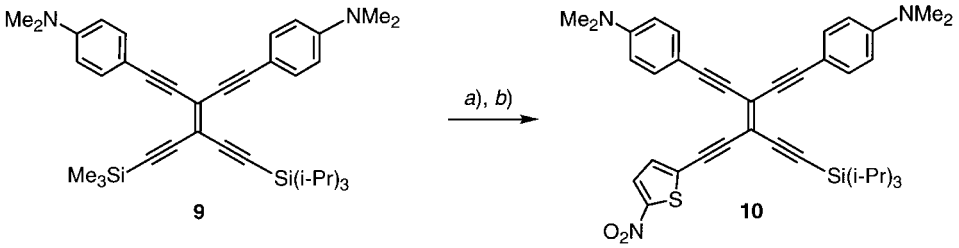

a) K_2CO_3, wet MeOH, THF, r.t., 2 h. *b*) 2-Iodo-5-nitrothiophene, $[PdCl_2(PPh_3)_2]$, CuI, NEt_3, r.t., 4 h; 45% (from **9**).

Protodesilylation of bis-donor-substituted TEE **9** [5][6], followed by cross-coupling with 2-iodo-5-nitrothiophene yielded tris-arylated **10** as a deep-red solid (*Scheme 3*).

For the synthesis of the fully two-dimensionally conjugated [8] TEE **11**, the $(i\text{-}Pr)_3Si$ groups in bis-donor-substituted **12** [5][6] were removed with Bu_4NF (*Scheme 4*). The resulting unstable diethynylated product was then quickly used, without isolation and purification, in the cross-coupling with 2-iodo-5-nitrothiophene to give **11** as a black solid that was only slightly soluble in polar organic solvents.

Scheme 4. Synthesis of Tetrakis-Arylated TEE **11**

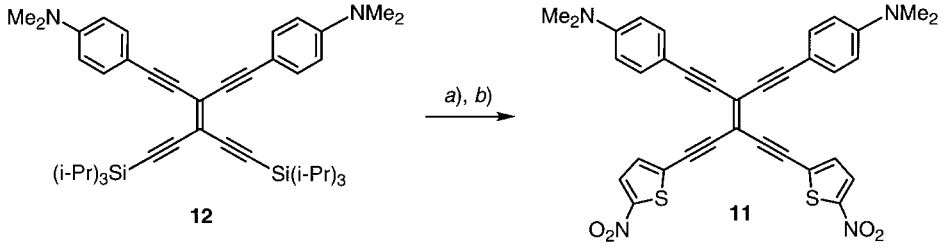

a) Bu_4NF, wet THF, r.t., 1 h. *b*) 2-Iodo-5-nitrothiophene, $[PdCl_2(PPh_3)_2]$, CuI, Et_3N, r.t., 16 h; 52% (from **12**).

The synthesis of dark-red tetrakis-arylated TEE **13**, featuring both 4-nitrophenyl and 5-nitro-2-thienyl acceptor moieties, was prepared by desilylation of tris-arylated **14** [5][6], followed by cross-coupling with 2-iodo-5-nitrothiophene (*Scheme 5*).

Scheme 5. *Synthesis of Tetrakis-Arylated TEE* **13**

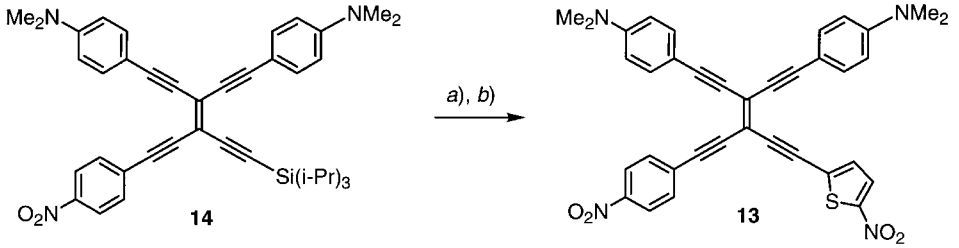

a) Bu_4NF, wet THF, r.t., 1 h. *b*) 2-Iodo-5-nitrothiophene, $[PdCl_2(PPh_3)_2]$, CuI, Et_3N, r.t., 4 h; 66% (from **14**).

Finally, we also prepared the dithienyl-substituted TEE **15** by protodesilylation of **16** [36], followed by cross-coupling with 2-iodothiophene. With its four *t*-Bu groups, compound **15** is highly soluble in organic solvents.

Scheme 6. *Synthesis of TEE* **15**

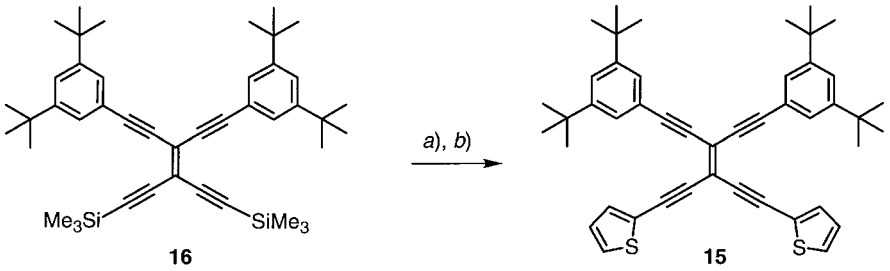

16 **15**

a) K_2CO_3, wet MeOH, THF, r.t., 2 h. *b*) *2*-Iodothiophene, $[PdCl_2(PPh_3)_2]$, CuI, Et_3N, r.t., 48 h; 15% (from **16**).

All nitrothienyl-substituted TEEs are stable in solution or as neat solids for months when exposed to air at room temperature. Melting (m.p.) and decomposition (d.p.) points for **2**, **5**, **6**, **10**, **11**, and **13** were determined by conventional melting-point determination and differential-scanning calorimetry (DSC), respectively. The data are summarized in *Table 1* together with those for the similarly substituted 4-nitrophenyl derivatives **14** and **17**–**20**. A comparison of the decomposition points shows that structurally related compounds in both series display quite similar stability.

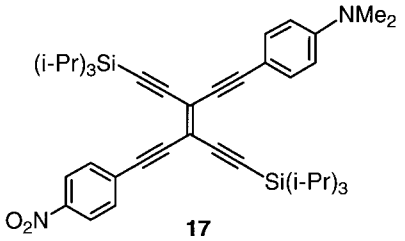

17

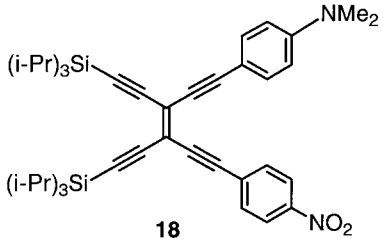

18

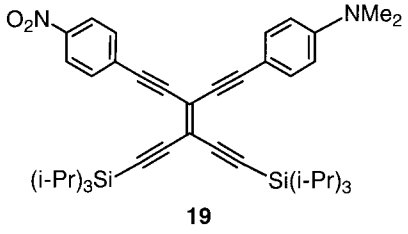

19

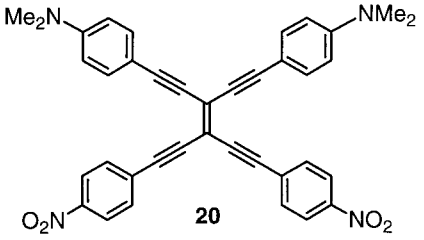

20

2.2. *X-Ray Crystal Structures.* The solid-state structures of four nitrothienyl-TEEs (**2**, **10**, **11**, and **13**) were determined by X-ray crystal-structure analysis. The compounds predominantly show a fully planar π-conjugated C-framework including both the TEE core and the appended aromatic rings. This is in agreement with previously reported X-

Table 1. *Melting- and Decomposition-Point Data for Selected Arylated Tetraethynylethenes*

Nitrothienyl-TEE	M.p. [°][a])	D.p. [°][b])	Nitrophenyl-TEE[c])	M.p. [°][a])	D.p. [°][b])
2	174–175	185	**17**	190–191	190
5	137–139	[d])	**18**	182–183	[d])
6	131–132, 142[b])	205[e])	**19**	129–130	210
10	158–159, 153[b])	172	**14**	169–170 (dec.)	165
11	[f])	210	**20**	247 (dec.)	240
13	210 (dec.)	223			

[a]) Uncorrected melting point. [b]) Differential scanning calorimetry (DSC). [c]) From [5]. [d]) Not performed. [e]) Slow decomposition from 205–230°. [f]) Not observed.

ray crystal structures of other D-A-substituted TEE derivatives [5][6]. The sole exception is observed for tris-arylated **10**, which shows one of the *N*,*N*-dimethylaniline groups rotated out of the molecular plane by *ca.* 90°. In this conformation, which is certainly due to crystal-packing effects, π-electron conjugation is maintained between this ring and the TEE core, as a result of the two orthogonal sets of π-bonds in the adjacent C≡C bond. In all four crystal structures, bond lengths and bond angles in the TEE core were in the range of those observed in previously studied derivatives [5][6], with little indication for intramolecular ground-state charge transfer. These findings are in accord with similar and independent investigations by *Brédas* and co-workers [37][38], and *Stiegman* and co-workers [39–41] on D-A-substituted α,ω-diphenylpolyynes, which showed little distortion of the C–C and C≡C bonds linking the donor and acceptor moieties.

The X-ray crystal structures of the four nitrothienyl-TEE derivatives are shown in *Figs. 1–4* together with selected bond lengths and bond angles. In the structure of **13**, disorder as described in the *Exper. Part* prevented refinement to a high level.

2.3. *Electronic Absorption Spectra.* The analysis of UV/VIS spectra provides a simple and expeditious manner of comparing electronic structure–property relationships in arylated TEEs. The electronic absorption characteristics of nitrothienyl-TEE derivatives are summarized in *Table 2* together with data for the analogous nitrophenyl derivatives **14** and **17**–**20** [5][6]. For bis-arylated TEEs, replacing the nitrophenyl with a nitrothienyl group induced a much larger spectral effect in the *cis*- than in the *trans*-series. Whereas the longest-wavelength absorption maximum (Band I, *Fig. 5*, top) shifted only by 8 nm upon changing from *trans*-D-A TEE **17** to nitrothienyl derivative

Table 2. *Maxima of the Longest-Wavelength Absorptions* λ_{max} [nm] *and Molar Extinction Coefficients* ε [M^{-1} cm^{-1}] *of Arylated Tetraethynylethenes in* $CHCl_3$

Nitrothienyl-TEE	Band II	Band I	Nitrophenyl-TEE[a])	Band II	Band I
2	361 (17900)	477 (32900)	**17**	352 (16300)	468 (31200)
5	400 (33500)	500 (14300)	**18**	371 (30700)	471 (17000)
6	400 (35700)	423 (33900)	**19**	373 (30100)	447 (19900)
10	391 (24100)	477 (34000), 530 (25200)[b])	**14**		461 (38200)
11	377 (30500)	498 (48400), 570 (33600)[b])	**20**		486 (40700)
13	356 (27700)[b])	484 (42000), 544 (33300)[b])			

[a]) From [5]. [b]) Shoulder.

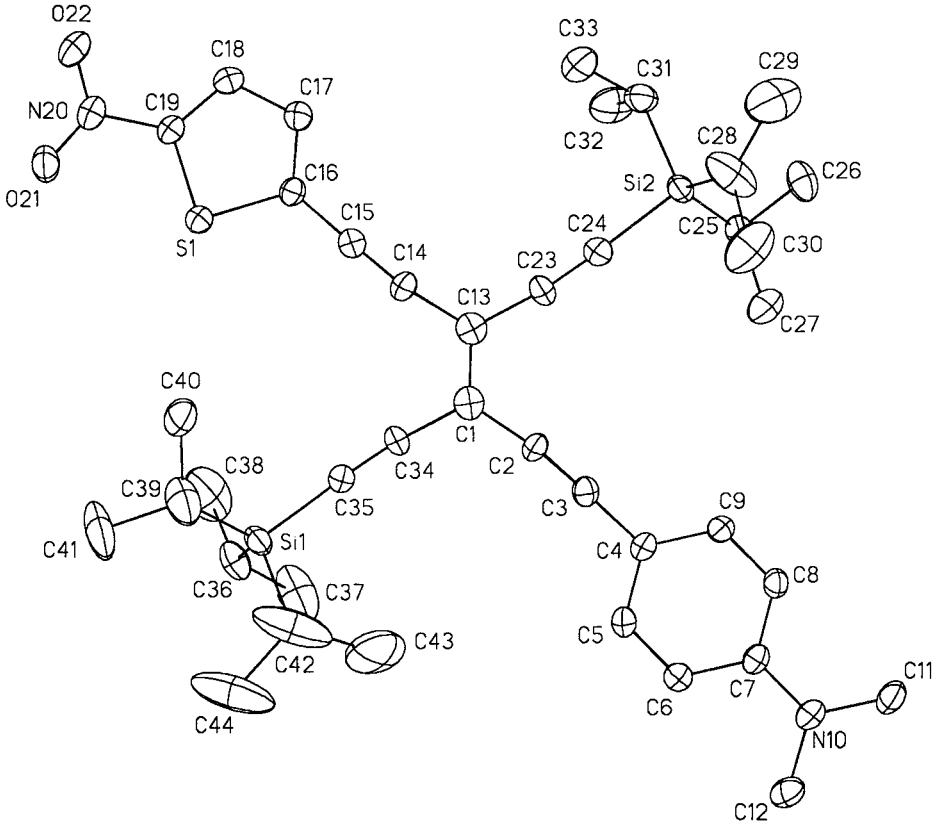

Fig. 1. *X-Ray crystal structure of* **2**. Arbitrary numbering. Atomic-displacement parameters obtained at 203 K are drawn at the 30% probability level. Selected bond lengths [Å] and angles [°]: C(3)–C(4) 1.434(5), C(2)–C(3) 1.204(5), C(1)–C(2) 1.426(6), C(1)–C(13) 1.344(6), C(13)–C(14) 1.430(6), C(14)–C(15) 1.204(5), C(15)–C(16) 1.414(5), C(13)–C(23) 1.439(6), C(23)–C(24) 1.197(5), C(24)–Si(2) 1.844(4), C(1)–C(34) 1.453(5), C(34)–C(35) 1.197(5), C(35)–Si(1) 1.845(4); C(2)–C(3)–C(4) 177.8(4), C(1)–C(2)–C(3) 172.1(4), C(2)–C(1)–C(13) 122.3(3), C(1)–C(13)–C(14) 120.6(3), C(13)–C(14)–C(15) 172.4(4), C(14)–C(15)–C(16) 177.8(4), C(1)–C(13)–C(23) 120.8(4), C(13)–C(23)–C(24) 173.4(4), C(23)–C(24)–Si(2) 176.4(4), C(2)–C(1)–C(34) 117.6(4), C(14)–C(13)–C(23) 118.5(4), C(1)–C(34)–C(35) 173.0(4), C(34)–C(35)–Si(1) 175.3(4).

2, the maxima of the two longest-wavelength bands (Bands I and II, *Fig. 5*, middle) both shifted by 30 nm to lower energy upon changing from *cis*-D-A-TEE **18** to **5**. The intramolecular charge-transfer character of the longest-wavelength absorption band in donor-acceptor-substituted TEEs had previously been demonstrated in great detail [5][6].

One of the most noticeable electronic characteristics of the *cis*-isomers **5** and **18**, in comparison to the *trans*-isomers **2** and **17**, is the difference in relative intensity of the central absorption peak (Band II). Whereas this band has the highest intensity in the spectra of **5** and **18**, its magnitude is greatly diminished in the corresponding *trans*-isomers. The origin of this difference can be convincingly accounted for by analysis of the transition dipoles calculated for these four molecules (*vide infra*).

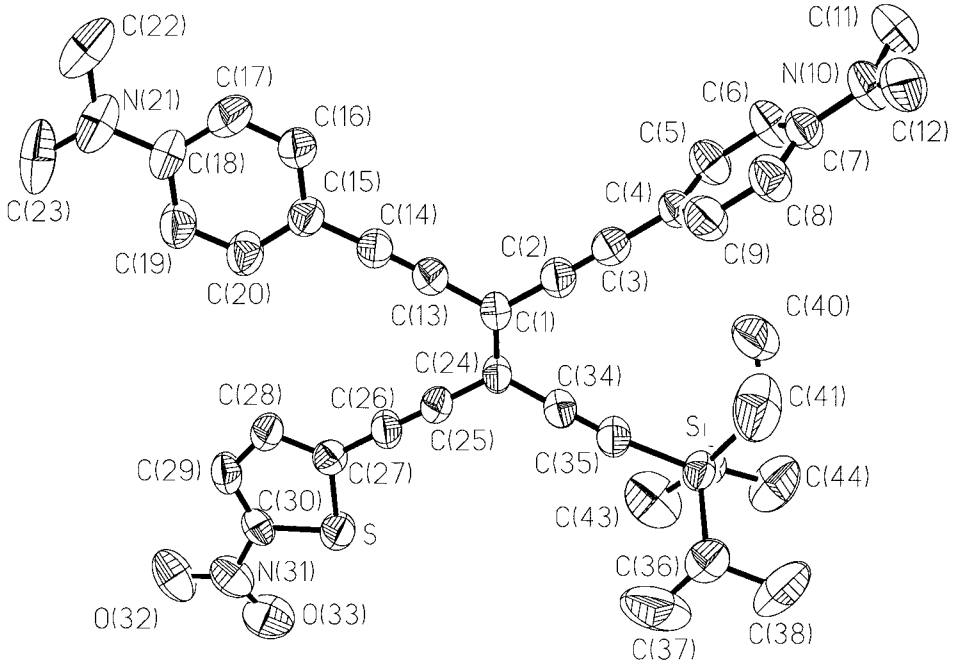

Fig. 2. *X-Ray crystal structure of* **10**. Arbitrary numbering. Atomic-displacement parameters obtained at 293 K are drawn at the 50% probability level. Selected bond lengths [Å] and angles [°]: C(3)–C(4) 1.438(9), C(2)–C(3) 1.201(8), C(1)–C(2) 1.416(9), C(1)–C(13) 1.433(10), C(13)–C(14) 1.193(9), C(14)–C(15) 1.433(10), C(1)–C(24) 1.379(9), C(24)–C(25) 1.415(5), C(25)–C(26) 1.202(8), C(26)–C(27) 1.407(9), C(24)–C(34) 1.425(9), C(34)–C(35) 1.207(9), C(35)–Si(1) 1.841(11); C(2)–C(3)–C(4) 179.3(5), C(1)–C(2)–C(3) 177.1(5), C(2)–C(1)–C(13) 117.5(4), C(1)–C(13)–C(14) 177.8(4), C(13)–C(14)–C(15) 178.2(5), C(2)–C(1)–C(24) 121.8(5), C(1)–C(24)–C(25) 121.0(5), C(24)–C(25)–C(26) 178.7(4), C(25)–C(24)–C(34) 118.3(4), C(25)–C(26)–C(27) 178.1(5), C(1)–C(24)–C(34) 120.7(4), C(24)–C(34)–C(35) 179.2(5), C(34)–C(35)–Si(1) 173.7(4).

The spectra of the two geminally bis-arylated TEEs **6** and **19**, with cross-conjugated D-A patterns, are remarkably different (*Fig. 5*, bottom). First, there is a 27-nm bathochromic shift of the central absorption band (Band II), resulting from thiophene substitution, from 373 nm for **19** to 400 nm for **6**. Even more remarkable is the change of the longest-wavelength absorption maximum (Band I) by 24 nm to higher energy upon substituting the nitrophenyl (**19**: 447 nm) by the nitrothienyl (**6**: 423 nm) moiety, whereas the molar absorptivity of this band in **6** ($\varepsilon = 33900\text{M}^{-1}\,\text{cm}^{-1}$) is nearly twice that in **19** ($\varepsilon = 19900\text{M}^{-1}\,\text{cm}^{-1}$). The end absorption of **6**, on the other hand, appears at lower energy (*ca.* 35 nm) than that of **19**.

Experimentally, third-harmonic-generation studies showed **6** to be a better NLO chromophore, with a higher second hyperpolarizability γ than **19** [8][11][13]. Thus, the increased oscillator strength of the main bands in **6**, seems to impact the second hyperpolarizability and the nonlinear optical response to a larger extent than the shift of the lowest-wavelength absorption maximum (Band I) to higher energy [42].

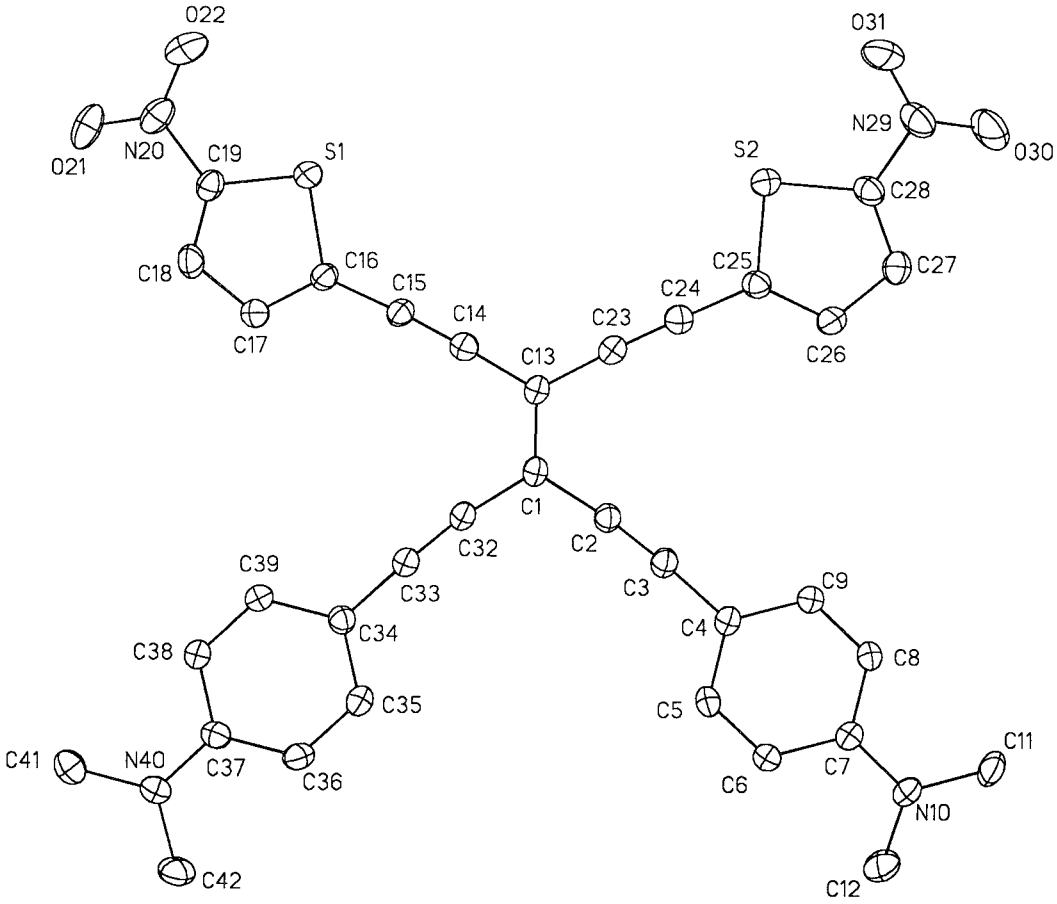

Fig. 3. *X-Ray crystal structure of* **11**. Arbitrary numbering. Atomic-displacement parameters obtained at 223 K are drawn at the 50% probability level. Selected bond lengths [Å] and angles [°]: C(3)–C(4) 1.422(4), C(2)–C(3) 1.201(4), C(1)–C(2) 1.414(4), C(1)–C(13) 1.389(4), C(13)–C(14) 1.416(4), C(14)–C(15) 1.201(4), C(15)–C(16) 1.406(4), C(13)–C(23) 1.418(4), C(23)–C(24) 1.205(4), C(24)–C(25) 1.415(4), C(1)–C(32) 1.418(4), C(32)–C(33) 1.205(4), C(33)–C(34) 1.422(4); C(2)–C(3)–C(4) 175.7(3), C(1)–C(2)–C(3) 174.2(3), C(2)–C(1)–C(13) 122.3(2), C(1)–C(13)–C(14) 120.6(2), C(13)–C(14)–C(15) 177.2(3), C(14)–C(15)–C(16) 177.0(3), C(1)–C(13)–C(23) 119.3(2), C(13)–C(23)–C(24) 176.9(3), C(23)–C(24)–C(25) 179.2(3), C(2)–C(1)–C(32) 115.0(2), C(14)–C(13)–C(23) 120.0(2), C(1)–C(32)–C(33) 171.3(3), C(32)–C(33)–C(34) 177.4(3).

The maximum of the longest-wavelength absorption band of the tris-arylated nitrothienyl derivative **10** (477 nm) is shifted bathochromically by 16 nm as compared to nitrophenyl derivative **14** (461 nm; *Fig. 6*, top). Furthermore, an additional shoulder at lower energy (*ca.* 530 nm) appears in the spectrum of **10** and the end-absorption is shifted to lower energy as well. These lower-energy absorption characteristics presumably manifest themselves in the NLO studies, where an increased γ value was measured for **10** as compared to **14** [11][13].

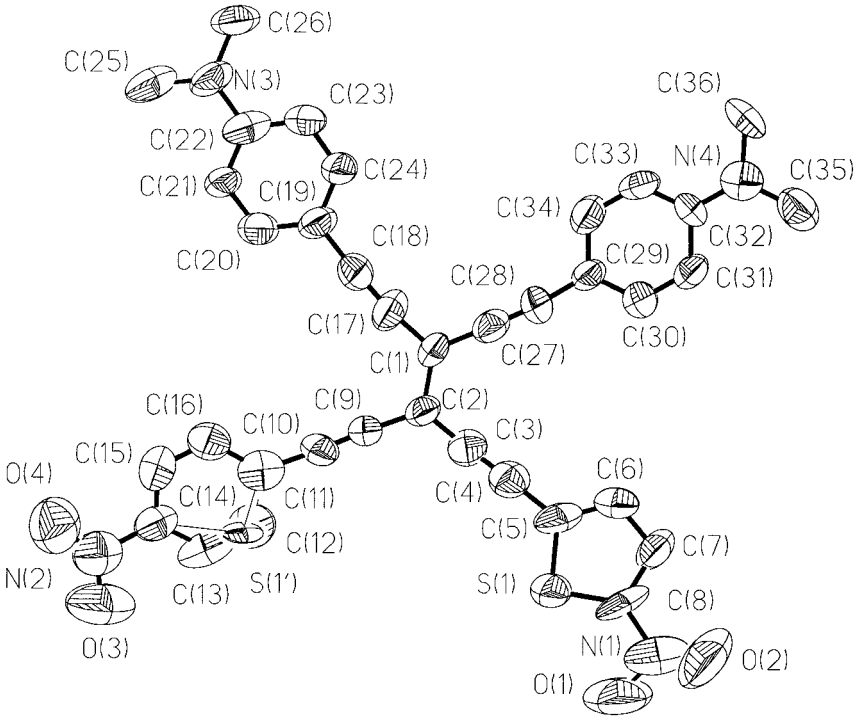

Fig. 4. *X-Ray crystal structure of* **13**. Arbitrary numbering. Atomic-displacement parameters obtained at 293 K are drawn at the 50% probability level. Selected bond lengths [Å] and angles [°]: C(4)–C(5) 1.446(13), C(3)–C(4) 1.218(13), C(2)–C(3) 1.355(12), C(1)–C(2) 1.428(14), C(2)–C(9) 1.422(15), C(9)–C(10) 1.145(16), C(10)–C(11) 1.438(16), C(1)–C(17) 1.376(13), C(17)–C(18) 1.218(12), C(18)–C(19) 1.464(13), C(1)–C(27) 1.455(15), C(27)–C(28) 1.181(15), C(28)–C(29) 1.395(16); C(3)–C(4)–C(5) 178.4(11), C(2)–C(3)–C(4) 176.5(11), C(1)–C(2)–C(3) 119.6(9), C(1)–C(2)–C(9) 119.3(7), C(3)–C(2)–C(9) 121.0(9), C(2)–C(9)–C(10) 175.3(9), C(9)–C(10)–C(11) 176.2(8), C(2)–C(1)–C(17) 121.6(9), C(1)–C(17)–C(18) 170.9(11), C(17)–C(18)–C(19) 174.9(11), C(2)–C(1)–C(27) 122.6(7), C(1)–C(27)–C(28) 176.7(8), C(27)–C(28)–C(29) 173.4(11), C(17)–C(1)–C(27) 115.7(9).

Clear electronic changes due to the substitution of nitrophenyl by nitrothienyl rings are also apparent in the series of tetrakis-arylated TEEs (*Fig. 6*, bottom). The maximum of the lowest-wavelength absorption band steadily decreases in energy and increases in absorptivity upon changing from **20**, to **13**, and to **11**. At the same time, upon stepwise introduction of the nitrothienyl rings, the shoulder at lower energy becomes increasingly pronounced, and the end absorption shifts bathochromically. Another interesting feature develops with increasing nitrothienyl substitution in the higher-energy spectral region: Whereas nitrophenyl derivative **20** shows a minimum around 370–380 nm, mono-nitrothienyl derivative **13** displays a shoulder and bis-nitrothienyl derivative **11** a distinct new band at 377 nm. Overall, the comparative analysis of the electronic absorption characteristics clearly demonstrates that nitrothienyl substitution profoundly and differentially affects donor-acceptor conjugation characteristics in multiply arylated TEEs.

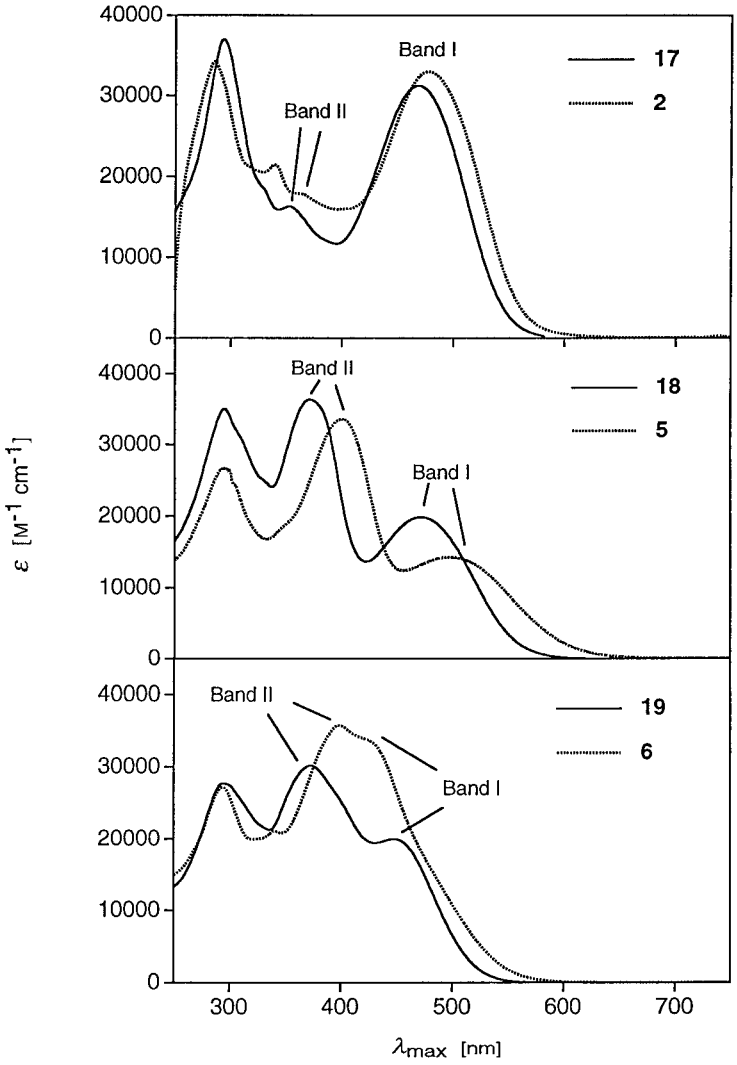

Fig. 5. *Electronic absorption spectra in $CHCl_3$ of bis-arylated TEEs with nitrothienyl and nitrophenyl groups*

2.4. *Electrochemical Investigations.* The electrochemical behavior of the nitrothienyl-substituted TEEs was studied in 0.1M Bu_4NPF_6 in CH_2Cl_2 on a glassy carbon working electrode as summarized in *Table 3*. For comparison purposes, the nitrophenyl derivative **20** was also included. All potentials were referenced *vs.* the ferrocene/ferricinium couple (Fc/Fc^+), which was used as an internal standard in all experiments.

The behavior of nitrothienyl-TEEs mirrors that of the previously studied nitrophenyl derivatives [7]; namely the different nitrothienyl moieties behave essentially as independent redox centers. That is to say that, after the first electron transfer has occurred, additional redox sites present in the molecule are not influenced, and

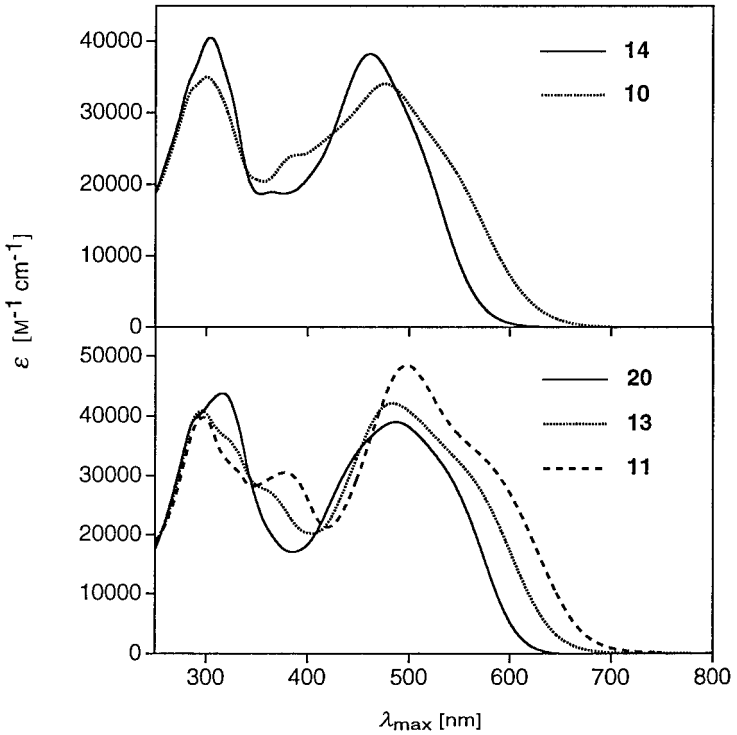

Fig. 6. *Electronic absorption spectra in $CHCl_3$ of tris- and tetrakis-arylated TEEs with nitrothienyl and nitrophenyl groups*

subsequent reductions occur at potentials expected in the absence of any other functionality. The nitrothienyl groups uniformly undergo reversible one-electron reductions at −1.23 V. For the non-symmetrically substituted TEE **13**, the reduction of the nitrothienyl moiety is followed by a second one-electron transfer to the nitrophenyl group at −1.40 V. This reduction potential is identical to that observed for the nitrophenyl-TEEs such as **20**, as previously studied [7]. For **13**, the difference in the reduction potential observed for the nitrophenyl (−1.40 V) and nitrothienyl (−1.23 V) groups is equal to 170 mV. This is in excellent agreement with the redox data reported for the independent reduction, in DMF, of 4-nitrobenzene (−1.60 V *vs.* Fc/Fc^+) and 2-nitrothiophene (−1.43 V *vs.* Fc/Fc^+) [43].

Following reduction of the nitroaryl groups, the nitrothienyl-containing TEEs all experience a one-electron reduction of the TEE core, which occurs between −1.60 and −1.64 V. The TEE-core-centered reduction of the nitrothienyl derivatives is, therefore, facilitated as compared to that of the analogous nitrophenyl derivatives (*e.g.*, −1.69 V in **20**). This exemplifies the ability of the nitrothienyl group to better participate in charge delocalization and thus, reduce the electron density of the TEE framework when compared with the nitrophenyl group.

The electrochemical analysis of **15** showed one reversible reduction at −1.68 V and one quasi-reversible oxidation step at +0.88 V (oxidation of the thiophene). In

Table 3. *Electrochemical Data for Arylated Tetraethynylethenes*[a])

Compound	Cyclic voltammetry			Rotating-disk electrode		
	E'^0 *vs.* Fc [V][b])	ΔE_p [mV][c])	E_{pc} *vs.* Fc [V][d])	$E_{1/2}$ *vs.* Fc [V]	Slope [mV][e])	No. of electrons
2	−1.23	90		−1.25	90	1
	−1.63	80		−1.67	70	1
	+0.47	76		+0.47	64	1
			+1.21	+1.19	63	1
10	−1.23	105		−1.23	72	1
	−1.63	104		−1.66	64	1
			+0.47	+0.46	105	2
11	−1.22	120		−1.22		[f])
	−1.60	90		[g])		
			−2.14			
			+0.48	[f])		
13	−1.22	80		−1.21	65	1
	−1.40	75		−1.42	68	1
	−1.64	80		−1.65	68	1
				−2.15	140	
			+0.47	+0.46	71	[f])
15	−1.68	71				
	+0.88	100				
20[h])	−1.38	80		−1.42	86	2
	−1.69	105		−1.76	65	1
			−2.11	−2.17	113	1
			+0.46	+0.42	60[i])	2

[a]) Redox potentials observed in 0.1M Bu_4NPF_6 in CH_2Cl_2 on glassy carbon electrode. [b]) Formal redox potential $E'^0 = (E_{pa} + E_{pc})/2$. [c]) At scan rate of 100 mV s^{-1}. [d]) Peak potentials for irreversible reductions and oxidations. [e]) Logarithmic analysis of the wave obtained by plotting E *vs.* $\log[I/I_{lim} - I)]$. [f]) Polarographic maximum. [g]) Poorly resolved wave. [h]) From [7]. [i]) Adsorption.

contrast to nitrothienyl derivatives, where the first reduction occurs at the nitroaryl group, the first (and only) reduction event for **15** corresponds to an electron transfer directly to the TEE core. In combination with the data for TEEs **2**, **10**, **11**, and **13**, this confirms that the second electron transfer observed at *ca.* −1.6 V does indeed occur in the TEE core of these nitrothienyl derivatives. In attempts to exploit the well-established ability of thiophenes to engage in electrochemical polymerization in the absence of substituents in the 2-position, TEE **15** was investigated by iterative cyclic voltammetry between 0 and +1.2 V. Unfortunately, no evidence of polymerization was observed.

The oxidation of the *N*,*N*-dimethylaniline moieties in the D-A-substituted TEEs was affected neither by the presence of one or two nitrothienyl groups nor by the presence of mixed nitrophenyl and nitrothienyl acceptors, as in **13**. Thus, all *N*,*N*-dimethylaniline groups are oxidized at *ca.* +0.46 V, in accord with previously reported oxidation potentials for D-A-substituted TEEs such as **20** [7].

2.5. *Computational Studies.* 2.5.1. *Methods.* For the computation of the excitation energies and the transition dipole moments, a single configuration interaction (SCI) method based on the INDO/S Hamiltonian (Intermediate Neglect of Differential Overlap/Spectroscopic Parametrization) as implemented in the programs ZINDO [44] and *Gaussian 94* [45] was used. The molecular geometries were obtained from AM1

(Austin Model 1) calculations performed with MOPAC [46]. The molecular orbitals were visualized with the MOLEKEL [47] post-processing tool.

The active space for the SCI calculations included the 20 highest-occupied and the 20 lowest-unoccupied orbitals. Validation studies of this computational model showed that the active space is sufficiently large, and that the inclusion of higher excitations has no significant effect on the computed result. Similarly, the use of molecular geometries obtained from *Hartree-Fock* calculations did not have an impact on the computed spectra. This computational model had been used previously in similar studies by us [33] and others [48].

2.5.2. *Analysis of Spectral Features.* All empirical features of relevance in the experimental UV/VIS spectra for **2**, **5**, **6**, and **17**–**19** are correctly reproduced by computation. The computed spectra predict a bathochromic shift for Band I upon replacement of the nitrophenyl group with a nitrothienyl group (*Table 4*), which is experimentally observed in the series of *trans*- and *cis*-bis-arylated compounds (*Fig. 5*, top and middle). The relative intensities of Bands I and II are also correctly reproduced in each case. Contrary to experiment, however, the bathochromic shift of Band I is predicted to be much stronger for **2** and **5**. Furthermore, a bathochromic shift of Band I

Table 4. *INDO/SCI-Computed Absorption Maxima* λ [nm], *Oscillator Strengths* f (in Arbitrary Units), *and Principal Configurations with CI Expansion Coefficients of Bands I and II of Nitrophenyl-TEEs* **17**–**19** *and Nitrothienyl-TEEs* **2**, **5**, *and* **6**. H = HOMO, L = LUMO, CI = Configuration Interaction.

TEE	Band	λ (nm)	f	Principal configurations, CI expansion coefficients
17	I	413	1.44	−0.72 [H → L]
				−0.55 [H → L + 1]
	II[a])	334	0.03	0.67 [H → L + 1]
				−0.40 [H − 1 → L]
18	I	422	0.78	−0.76 [H → L]
				−0.52 [H → L + 1]
	II	336	0.68	−0.72 [H → L + 1]
				−0.40 [H − 1 → L]
19	I	391	0.78	−0.68 [H → L]
				0.56 [H → L + 1]
	II	351	0.96	0.59 [H → L + 1]
				−0.50 [H − 1 → L]
2	I	466	1.47	−0.82 [H → L]
				−0.39 [H − 1 → L]
	II[a])	359	0.06	0.76 [H → L + 1]
				−0.40 [H − 1 → L]
5	I	490	0.53	−0.86 [H → L]
				−0.32 [H − 1 → L]
	II	361	1.15	0.71 [H → L + 1]
				0.49 [H − 1 → L]
6	I	441	0.79	0.72 [H → L]
				−0.60 [H − 1 → L]
	II	372	1.03	−0.69 [H → L + 1]
				−0.43 [H − 1 → L]

[a]) Band of *trans*-isomers with very weak intensity that could not be detected graphically, but only by numerical inspection of the transition energies data (*cf.* text).

is also predicted for geminally disubstituted **6**, in contrast to the experimentally observed hypsochromic shift.

It is interesting to note that the deviations between computed and experimental absorption frequencies appear to be characteristic of the type of substituent (nitrophenyl *vs.* nitrothienyl) rather than for the substitution pattern (*trans*, *cis*, or geminal). For the three nitrophenyl derivatives **17**–**19**, the computed absorption wavelength is predicted to be shorter by 53 ± 4 nm for Band I, and by 25 ± 10 nm for Band II. For the nitrothienyl derivatives **2**, **5**, and **6**, the average deviation is considerably smaller, but no longer as systematic: the bands are predicted to occur at shorter wavelengths by 1 ± 17 (Band I) and 23 ± 21 nm (Band II). It should be pointed out, however, that the computed spectra were *not* corrected for solvent effects, which will, to an unknown extent, account for the deviations between computation and experiment.

If we correct the computed absorption wavelengths by these systematic deviations, *i.e.*, by red-shifting the computed wavelength of Bands I and II by 53 and 25 nm for the nitrophenyl derivatives, and by 1 and 23 nm for the nitrothienyl derivatives, the computed results compare very well with experiment. The effects of the change from nitrophenyl to nitrothienyl are now largest for the *cis*-compounds **5** and **18** for which a bathochromic shift of 16 nm is predicted, whereas the bands of the *trans* (**2** and **17**) and the geminal compounds (**6** and **19**) show only marginal bathochromic (1 nm) and hypsochromic (2 nm) shifts, respectively. In agreement with experiment, the *trans*-derivatives **2** and **17** are predicted by calculations to show the most intense lowest-energy absorption bands (Band I). Band II, on the other hand, is of much lower intensity for both **2** and **17** in both computation and experiment.

The computations reveal distinct preferences for one of the two possible orientations of the thienyl ring located in the TEE plane. Apparently, the thienyl S-atom in the *trans*-derivative **2** points towards the adjacent geminally oriented acetylenic arm of the TEE, in the *cis*-derivative **5** towards the donor substituent, and in the gem-derivative **6** towards the neighboring *cis*-oriented acetylenic arm. These structural conclusions were drawn from the comparison of the intensities of Bands I and II computed for the various conformers. The comparison based on the total energies does not allow for such distinctions as the energy differences between the two orientations are very small for all three derivatives.

Band I of the nitrophenyl derivatives **17**–**19** is composed principally of excitations from the HOMO into the LUMO ($H \rightarrow L$) and from the HOMO into the next higher virtual orbital ($H \rightarrow L+1$; see *Table 4* and *Fig. 7*). In the nitrothienyl compounds **2**, **5**, and **6**, the latter excitation is replaced by an excitation from the HOMO -1 to the LUMO ($H-1 \rightarrow L$). Band II for all compounds considered here (**2**, **5**, **6**, and **17**–**19**) shows the same composition, namely significant contributions from the $H \rightarrow L+1$ and $H-1 \rightarrow L$ transitions. The $H-1 \rightarrow L$ transition thus contributes to both Band I and II in the nitrothienyl compounds.

The orbital representations for the HOMO, HOMO -1, LUMO, and LUMO $+1$ are shown in *Fig. 7* for the *trans*-derivatives **2** and **17**. With one exception, the effect on the shape of these orbitals upon changing the acceptor substituent is small. The HOMO -1 of the nitrothienyl derivative **2** shows much greater delocalization, including significant charge on the thiophene ring. The same orbital of the nitrophenyl derivative **17** is less delocalized and shows no amplitude on the nitrophenyl unit.

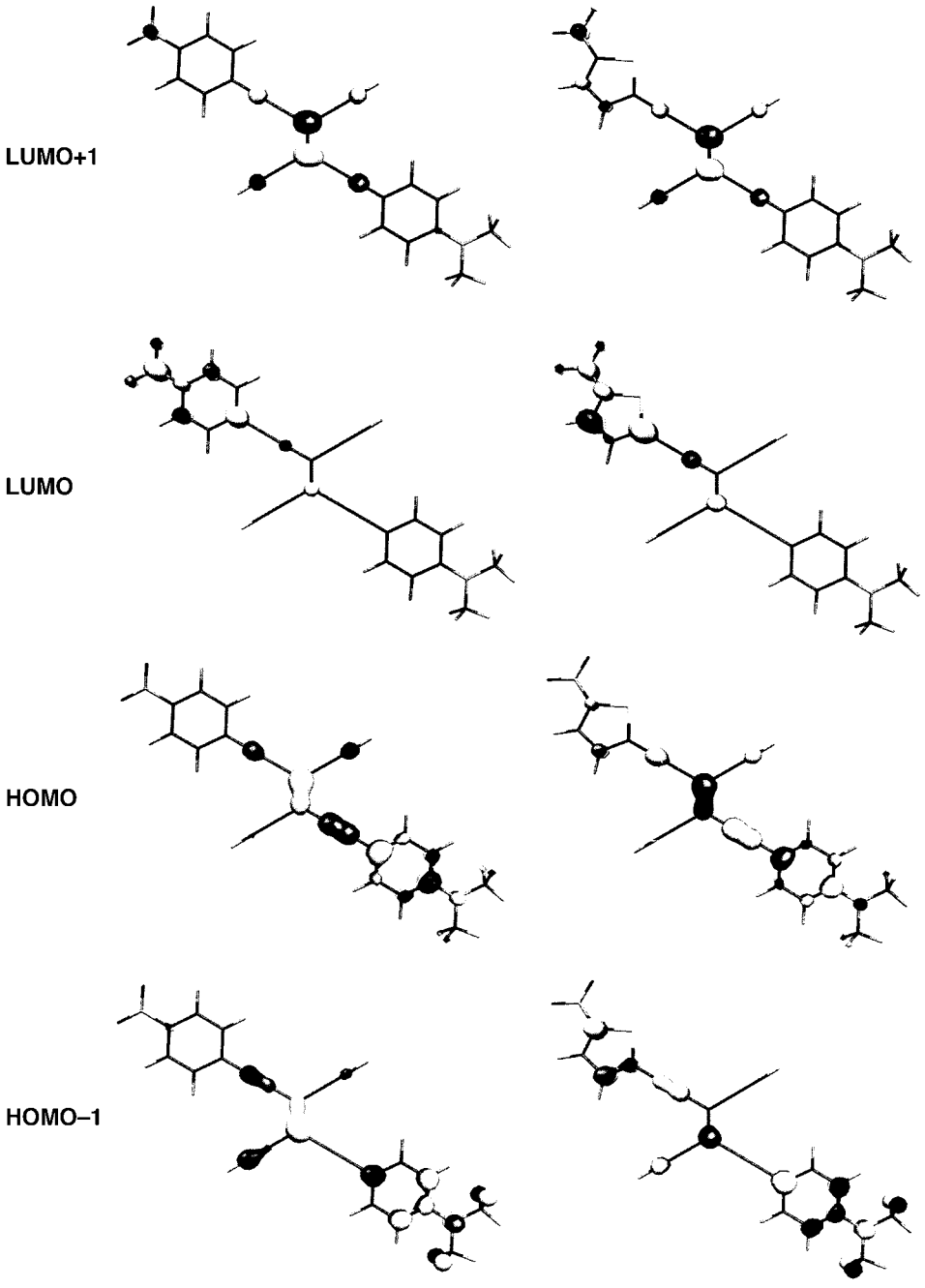

Fig. 7. *Molecular orbitals for* trans-*bis-arylated* **2** (right) *and* **17** (left)

Overall, the HOMO-LUMO gap for the nitrothienyl TEEs **2**, **5**, and **6** is reduced by *ca.* 0.2 eV as compared to the gap for the nitrophenyl TEEs **17**–**19**, regardless of the substitution pattern. This change is due *entirely* to a lowering of the orbital energies of the LUMOs of the nitrothienyl compounds.

A summary of the transition dipoles M and related quantities for **2**, **5**, **6**, and **17**–**19** is provided in *Table 5*. Their inspection offers an explanation for the vastly different intensities of the absorption bands observed as a function of the substitution pattern (*cis*, *trans*, or geminal). This is discussed in the following for the two *trans*-derivatives **2** and **17**.

Table 5. *The Calculated Transition Dipole-Moment Vectors* M, *Their Norm* $\|M\|$, *and the Corresponding Unitary Vectors* $M/\|M\|$ *for the Principal Excitations Responsible for Bands I and II of TEE Derivatives by the INDO/S Method.* The quantity ρ represents the angle between the transition dipole vector M and the ground state dipole vector μ (in units of degrees; see also *Fig. 8*). INDO/S = Intermediate Neglect of Differential Overlap/Spectroscopic Parametrization.

TEE	Singly Excited Configuration	M	$\|M\|$	$M/\|M\|$ [a])	ρ
17	[H → L]	(5.26, −5.10)	7.33	(0.72, −0.70)	11
	[H → L+1]	(6.59, −3.89)	7.65	(0.86, −0.51)	24
	[H−1 → L]	(2.90, −1.86)	3.44	(0.84, −0.54)	22
18	[H → L]	(5.24, −1.67)	5.50	(0.95, −0.30)	11
	[H → L+1]	(−6.74, −3.61)	7.65	(−0.88, −0.47)	56
	[H−1 → L]	(−2.89, 4.65)	5.47	(−0.53, 0.85)	30
19	[H → L]	(−4.08, 1.21)	4.26	(−0.96, 0.28)	60
	[H → L+1]	(6.70, 3.59)	7.60	(0.88, 0.47)	75
	[H−1 → L]	(3.73, −4.97)	6.21	(0.60, −0.80)	24
2	[H → L]	(−7.05, 6.26)	9.43	(−0.75, 0.66)	13
	[H → L+1]	(−5.18, 3.60)	6.31	(−0.82, 0.57)	6
	[H−1 → L]	(−4.02, 2.23)	4.60	(−0.87, 0.48)	0
5	[H → L]	(−5.23, 2.89)	5.97	(−0.87, 0.48)	53
	[H → L+1]	(6.41, 4.20)	7.66	(0.84, 0.55)	65
	[H−1 → L]	(−2.21, 6.93)	7.27	(−0.30, 0.95)	9
6	[H → L]	(−4.65, 2.43)	5.25	(−0.89, 0.46)	75
	[H → L+1]	(−6.62, −3.83)	7.65	(−0.86, −0.50)	48
	[H−1 → L]	(3.41, −7.03)	7.81	(0.44, −0.90)	38

[a]) The unitary vector is reported in order to facilitate the numerical comparison between the transition-moment directions of the different configurations.

The transition dipole vectors of the two principal excitations responsible for Band I in the two *trans*-derivatives, *i.e.*, the H → L and H → L+1 excitations (H = HOMO, L = LUMO) for **17**, and the H → L and H−1 → L excitations for **2** are nearly parallel, showing an inclination angle ϕ of only 13° for both compounds (*Fig. 8* and *Table 5*; note that the angle ρ (see *Fig. 8*, lower right) in *Table 5* represents the inclination angle between the ground-state dipole vector and the transition dipole vector of the excitation considered). The inclination angle ϕ (see *Fig. 8*, upper right) is the difference between the values of ρ for the H → L and H → L+1 excitations for **17**, *i.e.*, 11° and 24°, and for the H → L and H−1 → L excitations for **2**, *i.e.*, 13° and 0° (see *Fig. 8*, upper right). As these two excitations enter the CI vector of the first-excited-state wavefunction with equal signs ('in phase'; see *Table 4*), a large transition dipole vector M results, explaining the high oscillator strength observed for Band I of the two *trans*-derivatives.

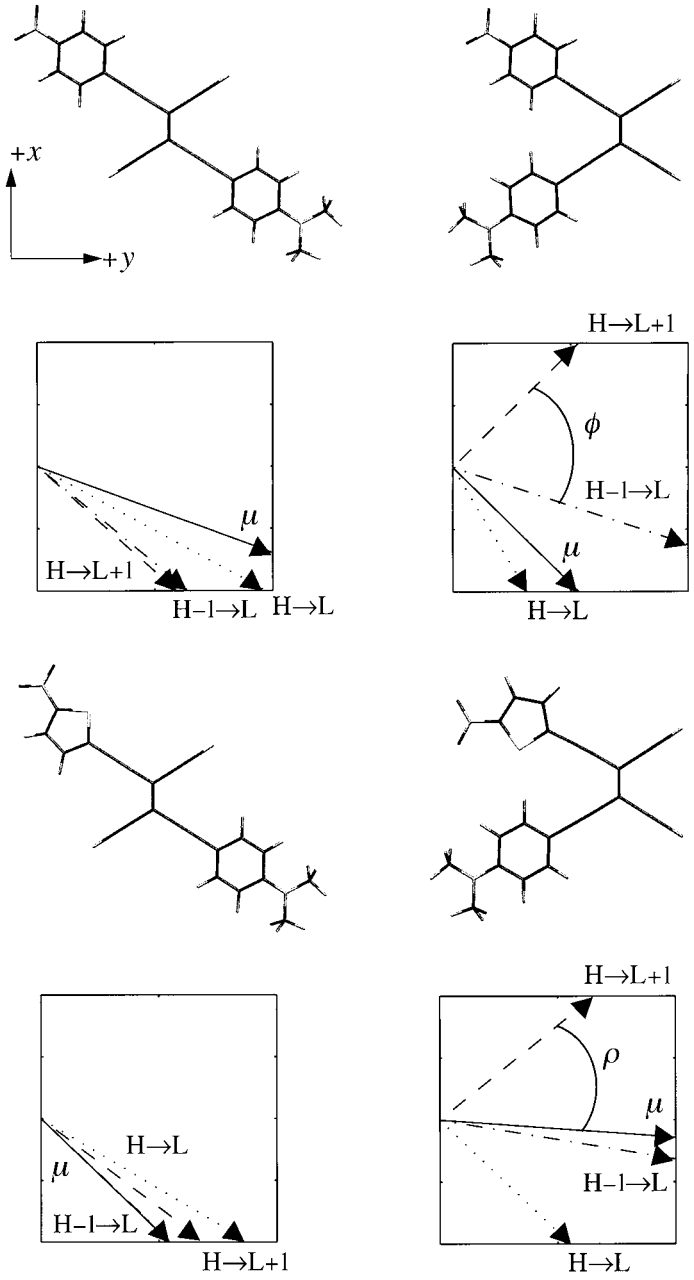

Fig. 8. *The calculated ground-state dipole vector* μ (solid line) *and the transition dipole vectors for the excitations* $H \rightarrow L$ (dotted line), $H \rightarrow L+1$ (dashed line), *and* $H-1 \rightarrow L$ (dashed-dotted line) *for the TEE derivatives* **17** (upper left), **18** (upper right), **2** (lower left), *and* **5** (lower right). The quantity ρ (lower right) indicates the angle between the ground-state-dipole and the transition-state-dipole vectors (see *Table 5* for complete listing), whereas ϕ shows the inclination angle between transition dipole vectors (see upper right; the example chosen is the inclination angle between the transition dipoles of the excitations responsible for Band II in **18**). Only the direction of each vector is shown. For their norm, see *Table 5*. H = HOMO, L = LUMO. The vectorial representation and the corresponding molecular structure are aligned in similar *x*,*y*-coordinate systems.

Band II is made up of the same set of excitations for all compounds (*Table 4*). As discussed earlier, it is composed of $H \rightarrow L+1$ and $H-1 \rightarrow L$ transitions. There is, however, one remarkable difference that explains the low intensity of Band II in the *trans*-substituted TEEs **2** and **17**. As in Band I, the transition dipole vectors for the two dominant excitations responsible for Band II are nearly parallel (inclination angles ϕ of 6° and 2°, respectively; see *Table 5* and *Fig. 8*). In the case of Band II, however, these two excitations enter the CI-vector of the excited-state wavefunction with *opposite* signs ('out of phase'; see *Table 4*). The resulting transition dipole moment therefore nearly vanishes, thus explaining the weak intensity of Band II observed for **2** and **17**.

A similar analysis can be made in order to explain the intensities of the bands of the *cis*- and geminal-derivatives as well, which show significant intensities for both Bands I and II.

2.5.3. *Electronic-Structure Considerations.* The analysis of the ground- and excited-state wavefunctions reveals some interesting detail about the role of the nitrothienyl unit that acts as a strong acceptor group, but at the same time features donor character with its electron-rich thiophene ring [14][15]. In general, the HOMO and HOMO -1 of the nitrophenyl compounds **17**–**19** show no significant amplitude on the acceptor group; *i.e.*, all charge is localized on the donor group and on the TEE backbone. The HOMO -1 of nitrothienyl compounds **2**, **5**, and **6**, however, shows considerable amplitude even on the thiophene rings. Despite this accumulation of valence charge on the acceptor unit for **2**, **5**, and **6** (*Fig. 7*), the LUMO energies are still lower than those of the nitrophenyl compounds, thus pointing at the enhanced acceptor capabilities of the nitrothienyl group.

In the first excitation (Band I), the amount of charge transferred to the nitrothienyl group of **2**, **5**, and **6** is slightly larger than that transferred to the nitrophenyl substituent of **17**–**19** (0.30 *vs.* 0.20 electrons in terms of *Mulliken* charges on average for all three isomeric series, *i.e.*, *cis*, *trans*, and geminal). For **2**, **5**, and **6**, however, the incoming charge is more strongly localized on the NO_2 group rather than on the thiophene ring. For the second excitation (Band II) of **2**, **5**, and **6**, a slight depopulation of the thiophene ring is observed (*ca.* 0.10 electrons), concurrent with a strong overall increase in the electron population on the NO_2 group (*ca.* 0.20 electrons).

On the donor side, it is interesting to note that in the nitrothienyl derivatives the TEE backbone is depopulated more strongly in the first excitation (*ca.* 0.20 electrons) than the dimethylaniline donor (*ca.* 0.10 electrons). The amount of charge withdrawn from the *N*,*N*-dimethylaniline group is very similar for both types of compounds. For the nitrophenyl compounds, a strong depopulation of the TEE backbone is observed in Band II. In that excitation, the TEE backbone of the nitrothienyl compounds appears as a weak acceptor (between 0.02 and 0.14 electrons, depending on the substitution pattern), whereas now the thiophene residue looses charge (see above).

Evidently, the delocalization of charge out of the TEE carbon framework is an important feature of the electronic structure of these D-A-functionalized molecules. The amount of charge excited from the backbone also strongly depends on the substitution pattern (*trans*, *cis*, and geminal).

3. Conclusions. – A series of D-A-substituted tetraethynylethenes (TEEs) with 4-(dimethylamino)phenyl donor and 5-nitro-2-thienyl acceptor moieties were assembled

by Pd^0-catalyzed *Sonogashira* cross-coupling. Bis-arylated TEEs feature one (*trans*, *cis*, or geminal) conjugation path between donor and acceptor, whereas tris- and tetrakis-arylated derivatives are two-dimensionally conjugated molecules with several conjugation paths between donor and acceptor. The latter had previously been shown to give enhanced third-order nonlinear optical response [11][13]. The structure-property relationships for this new generation of D-A-substituted TEEs were explored and compared with those in a series of analogously substituted TEEs featuring nitrophenyl (instead of nitrothienyl) acceptor moieties. The melting/decomposition points of the nitrothienyl-substituted TEEs were found to be in a range similar to those previously determined for the nitrophenyl analogs. In particular, the tetrakis-arylated derivatives were found to be quite stable, with decomposition points well over 200°. Four X-ray crystal-structure analyses revealed predominantly a fully planar π-conjugated C-framework including both the TEE core and the appended aromatic rings. Nearly normal bond lengths and angles suggested little, if any, intramolecular donor-acceptor interactions in the ground state. Electrochemical investigations showed that the nitrothienyl groups behaved as independent redox centers, regardless of the number or type of other aryl substituents. Following reduction of the nitrothienyl group(s), an electron transfer to the TEE core was observed at a potential *ca.* 70–100 mV less negative than for the analogous nitrophenyl derivatives, clearly showing the ability of the thiophene ring to better participate in π-conjugation and charge delocalization. The UV/VIS spectra of the D-A-substituted TEEs with nitrothienyl acceptors consistently showed broad, low-energy charge-transfer (CT) absorptions that were notably more intense than those of comparable TEEs with nitrophenyl acceptors. An enhanced π-electron delocalization in tris- and tetrakis-arylated TEEs, resulting from substitution of nitrophenyl by nitrothienyl rings, was clearly revealed by the appearance of a new shoulder at longer wavelengths and a bathochromically shifted end absorption.

Quantum-chemical calculations for diarylated TEEs **2**, **5**, **6**, and **17**–**19** were undertaken to enhance the understanding of the key features of their absorption spectra and electronic structure. The calculations show that the high intensity observed for the longest-wavelength absorption (Band I) in the *trans*-derivatives is due to the small inclination angle ϕ of the transition dipole vectors of the excitations responsible for the band. The same consideration applies for Band II, except that here the CI coefficients of the relevant excitations have opposite signs ('out of phase'). The analysis of the electronic structure confirms that the nitrothienyl group acts as a strong electron acceptor, and that, at the same time, the electron-rich thiophene heterocycle is also involved as a donor in the electronic transitions of Band II. This dual role is indicative of its support of enhanced π-conjugation. The impact of the type of acceptor (nitrothienyl *vs.* nitrophenyl) and of substitution pattern (*cis*, *trans*, or geminal) is reflected by the response of the TEE backbone, which, depending on the situation, also has the capability to act as a donor or weak acceptor.

The present study clearly shows that conjugated thiophene linkers can easily be incorporated into the TEE framework and successfully used to manipulate molecular properties. This knowledge and that from concurrent NLO studies are now being used to guide further structural changes towards optimized NLO chromophores, as well as the assembly of oligomeric and polymeric systems.

This work was supported by the *Swiss National Science Foundation*, a grant from the *ETH Research Council*, a postdoctoral fellowship from the *U.S. Office of Naval Research* (to *R. R. T.*), and a grant from the University of Alberta. We thank *R. E. Martin* and *F. Cardullo* for high-field NMR measurements.

Experimental Part

General. Reagents and solvents were purchased reagent grade and used without further purification. Compounds **3**, **4**, **9**, **12**, and **14** [5][6], **7** [3], **16** [49], 4-ethynyl-*N*,*N*-dimethylaniline [35] and 2-iodo-5-nitrothiophene [32] were prepared according to literature procedures. All reactions were performed in standard glassware under an inert atmosphere of N_2. A positive pressure of N_2 was essential to the success of Pd^0-catalyzed reactions. Degassing of solvents was accomplished by vigorously bubbling N_2 through the soln. for at least 45 min. Anh. $MgSO_4$ was used as the drying agent after aq. workup. Evaporation and concentration *in vacuo* was performed at H_2O-aspirator pressure. Column chromatography (CC): SiO_2-*60* (230–400 mesh) from *E. Merck* or SiO_2-*H* from *Fluka*. TLC: glass sheets covered with SiO_2-*60* F_{254} from *E. Merck*; visualization by UV light or anisaldehyde stain. M.p.: *Büchi SMP-20* apparatus; uncorrected. DSC: *Dupont 900 Differential Thermal Analyzer*. UV/VIS Spectra: *Varian-Cary-5* spectrophotometer at r.t.; λ_{max} in nm (ε in M^{-1} cm^{-1}). IR Spectra (cm^{-1}): *Perkin-Elmer 1600-FTIR*. ^{1}H- and ^{13}C-NMR: *Bruker AMX-500*, *Varian Gemini-200* and *-300* instruments at r.t. in $CDCl_3$; solvent peaks (7.24 ppm for ^{1}H and 77.0 ppm for ^{13}C) as reference. MS (*m/z*): *VG-Tribrid* instrument for EI and a *VG-ZAB-2SEQ* instrument for FAB in a 3-nitrobenzyl-alcohol matrix. Elemental analyses were effected by the Mikrolabor in the Laboratorium für Organische Chemie at ETHZ.

Electrochemistry. The electrochemical experiments were carried out at $20 \pm 2°$ in CH_2Cl_2 containing 0.1M Bu_4NPF_6 in a classical three-electrode cell. The working electrode was a glassy-carbon-disk electrode used either motionlessly for CV (10 mV s^{-1} to 10 V s^{-1}) or as a rotating-disk electrode (RDE). All potentials in the present study are referenced to the ferrocene/ferricinium (Fc/Fc^+) couple, which was used as an internal standard. The auxiliary electrode was a Pt wire, and an Ag wire was used as a pseudo-reference electrode. The accessible range of potentials was +1.2 to −2.0 V *vs.* Fc/Fc^+ on the Pt electrodes and +1.2 to −2.2 V *vs.* Fc/Fc^+ on GC in CH_2Cl_2.

X-Ray Crystal Structure of **2**. Single crystals were grown by slow evaporation of a CH_2Cl_2/MeCN soln. at r.t. X-Ray crystal data for $C_{40}H_{54}N_2O_2SSi_2$ (M_r 683.1): triclinic space group $P\bar{1}$ (No. 2), $D_c = 1.13$ g cm^{-3}, $Z = 2$, $a = 8.629(2)$, $b = 11.078(3)$, $c = 22.379(4)$ Å, $\alpha = 83.37(2)°$, $\beta = 82.07(2)°$, $\gamma = 72.45(2)°$, $V = 2014(1)$ Å^3, CuK_α radiation, $\theta \leq 55°$, 5437 unique reflections, $T = 203$ K. The structure was solved by direct methods (SHELXS-86) and refined by full-matrix least-squares analysis (SHELXL-97) with an isotropic extinction coefficient and an exponentially modified weight factor with $r = 5$ Å^2 (heavy atoms anisotropic, H-atoms isotropic, whereby H-positions are based on stereochemical considerations). Final $R(F) = 0.062$, $wR(F^2) = 0.148$ for 471 variables and 4277 observed reflections with $I > 2\sigma(I)$. *Cambridge Crystallographic Data Centre* deposition No. CCDC-142188.

X-Ray Crystal Structure of **10**. Single crystals were grown by slow evaporation of a CH_2Cl_2/MeCN soln. at r.t. X-Ray crystal data for $C_{39}H_{43}N_3O_2SSi$ (M_r 645.9): triclinic space group $P\bar{1}$, $D_c = 1.157$ g cm^{-3}, $Z = 2$, $a = 10.91(6)$, $b = 12.85(5)$, $c = 14.62(5)$ Å, $\alpha = 72.6(3)°$, $\beta = 78.0(4)°$, $\gamma = 73.0(3)°$, $V = 1854(14)$ Å^3, MoK_α radiation, $3 \leq 2\theta \leq 40°$, 3493 unique reflections, $T = 293$ K. The structure was solved by direct methods (SHELXTL PLUS) and refined by full-matrix least-squares analysis based on 3493 independent F^2 data and 416 parameters using experimental weights; heavy atoms anisotropic, H-atoms fixed isotropic with positions calculated from stereochemical considerations. Final $R(F) = 0.037$ for 2705 observed reflections with $I > 2\sigma(I)$ and $wR(F^2) = 0.104$ for all independent data. *Cambridge Crystallographic Data Centre* deposition No. CCDC-142651.

X-Ray Crystal Structure of **11**. Single crystals were grown by slow evaporation of a CH_2Cl_2/MeCN soln. at r.t. Low-temperature X-ray crystal data for $C_{34}H_{24}N_4O_4S_2$ (M_r 616.7): triclinic space group $P\bar{1}$ (No. 2), $D_c = 1.37$ g cm^{-3}, $Z = 2$, $a = 7.751(2)$, $b = 14.022(4)$, $c = 14.220(2)$ Å, $\alpha = 94.18(2)°$, $\beta = 91.20(2)°$, $\gamma = 103.39(2)°$, $V = 1498(1)$ Å^3, CuK_α radiation, $\theta \leq 60°$, 4437 unique reflections, $T = 223$ K. The structure was solved by direct methods (SHELXS-86) and refined by full-matrix least-squares analysis (SHELXL-97) with an isotropic extinction coefficient and an exponentially modified weight factor with $r = 5$ Å^2 (heavy atoms anisotropic, H-atoms isotropic, whereby H-positions are based on stereochemical considerations). Final $R(F) = 0.048$, $wR(F^2) = 0.124$ for 422 variables and 3864 observed reflections with $I > 2\sigma(I)$. *Cambridge Crystallographic Data Centre* deposition No. CCDC-142189.

X-Ray Crystal Structure of **13**. Single crystals were grown by slow evaporation of a CH_2Cl_2/MeCN soln. at r.t. X-Ray crystal data for $C_{36}H_{26}N_4O_4S$ (M_r 610.7): triclinic space group $P\bar{1}$, $D_c = 1.305$ g cm^{-3}, $Z = 2$, $a =$

7.80(2), $b = 14.05(3)$, $c = 14.60(6)$ Å, $\alpha = 93.6(3)^\circ$, $\beta = 91.9(3)^\circ$, $\gamma = 102.9(2)^\circ$, $V = 1554(8)$ Å^3, CuK_α radiation, $3 \leq 2\theta \leq 100^\circ$, 3093 unique reflections, $T = 293$ K. The structure was solved by direct methods (SHELXTL PLUS) and refined by full-matrix least-squares analysis based on 3093 independent F^2 data and 436 parameters using experimental weights; heavy atoms anisotropic, H-atoms fixed isotropic with positions calculated from stereochemical considerations. Final $R(F) = 0.112$ for 1556 observed reflections with $I > 2\sigma(I)$ and $wR(F^2) = 0.346$ for all independent data. The structure is disordered: 30% of the molecules are rotated by 180° about the C(1)–C(2) direction as indicated in *Fig. 4*. *Cambridge Crystallographic Data Centre* deposition No. CCDC-142385.

Crystallographic data (excluding structure factors) for the structures reported in this paper have been deposited with the *Cambridge Crystallographic Data Centre*. Copies of the data can be obtained, free of charge, on application to the CCDC, 12 Union Road, Cambridge CB2 1EZ, UK (fax: +44 (1223) 336 033; e-mail: deposit@ccdc.cam.ac.uk).

General Workup for Pd^0-Catalyzed Alkynylations. Unless otherwise noted, Pd^0-catalyzed coupling reactions were worked up as follows. After reacting the aryl or vinyl halide with the terminal alkyne for the indicated time period, the solvent Et_3N was removed *in vacuo*. The resulting residue was dissolved in a minimal amount of CH_2Cl_2 and passed through a plug (SiO_2; CH_2Cl_2). The solvent was removed to give the crude product, which was then purified as described in the individual procedures.

(E)-1-[4-(Dimethylamino)phenyl]-6-(5-nitro-2-thienyl)-3,4-bis[2-(triisopropylsilyl)ethynyl]hex-3-ene-1,5-diyne (**2**). A mixture of **3** (40 mg, 0.064 mmol) and K_2CO_3 (10 mg, 0.07 mmol) in wet MeOH (15 ml) and THF (5 ml) was stirred at r.t. for 2 h. Et_2O and H_2O were added, the org. phase was separated, dried, evaporated to 5 ml, and added to Et_3N (15 ml). The soln. was degassed, 2-iodo-5-nitrothiophene (20 mg, 0.078 mmol), [$PdCl_2(PPh_3)_2$] (8 mg, 0.01 mmol), and CuI (4 mg, 0.02 mmol) were added, and the mixture was stirred at r.t. for 12 h. Workup and CC (SiO_2-*H*; hexane/CH_2Cl_2 2:1) afforded **2** (27 mg, 62%). R_f 0.5. Dark red solid. M.p. 174–175°. UV/VIS ($CHCl_3$): 286 (34200), 340 (21500), 361 (17900), 477 (32900). IR (CCl_4): 2944, 2200, 2167, 1600, 1522, 1333. ^{1}H-NMR (500 MHz, $CDCl_3$): 1.14 (*s*, 21 H); 1.15 (*s*, 21 H); 3.02 (*s*, 6 H); 6.63 (*d*, $J = 8.9$, 2 H); 7.09 (*d*, $J = 4.3$, 1 H); 7.36 (*d*, $J = 8.9$, 2 H); 7.81 (*d*, $J = 4.3$, 1 H). ^{13}C-NMR (125.8 MHz, $CDCl_3$): 11.3 (2×); 18.7 (2×); 40.0; 87.3; 88.1; 96.7; 102.6; 102.7; 103.0; 103.6; 103.6; 108.7; 111.5; 112.6; 120.6; 128.5; 130.6; 131.1; 133.42; 150.8; 151.2. EI-MS (70 eV): 682 (100, M^+). X-Ray analysis: see *Fig. 1*.

(Z)-1-[4-(Dimethylamino)phenyl]-6-(5-nitro-2-thienyl)-3,4-bis[2-2(triisopropylsilyl)ethynyl]hex-3-ene-1,5-diyne (**5**). A soln of **2** (6 mg, 0.009 mmol) in hexane (200 ml) was irradiated (366 nm) in a quartz flask for 2 h at r.t. Removal of the solvent and prep. TLC (SiO_2; hexane/CH_2Cl_2 2:1) gave **5** (4 mg, 67%) and recovered **2** (2 mg, 33%). R_f 0.3. Black solid. M.p. 137–139°. UV/VIS ($CHCl_3$): 300 (26300), 400 (33500), 500 (14300). IR (CCl_4): 2942, 2203, 2174, 2140, 1606, 1336, 1106. ^{1}H-NMR (500 MHz, $CDCl_3$): 1.12 (*s*, 21 H); 1.13 (*s*, 21 H); 3.02 (*s*, 6 H); 6.65 (*d*, $J = 9.1$, 2 H); 7.12 (*d*, $J = 4.3$, 1 H); 7.36 (*d*, $J = 9.1$, 2 H); 7.82 (*d*, $J = 4.3$, 1 H). ^{13}C-NMR (125.8 MHz, $CDCl_3$): 11.3 (2×); 18.7 (2×); 40.1; 87.5; 88.5; 97.3; 102.5; 102.7; 103.3; 103.6; 104.0; 108.6; 111.8; 112.3; 120.4; 128.6; 130.7; 131.1; 133.3; 150.9; 151.2. EI-MS (70 eV): 682 (100, M^+). HR-MS: 682.3441 (M^+, $C_{40}H_{54}Si_2N_2O_2S^+$; calc. 682.3444).

1-[4-(Dimethylamino)phenyl]-6-(triisopropylsilyl)-4-[2-(triisopropylsilyl)ethynyl]-3-[2-(trimethylsilyl)ethynyl]hex-3-ene-1,5-diyne (**8**). A mixture of **7** (0.255 g, 0.467 mmol), 4-ethynyl-*N*,*N*-dimethylaniline (73 mg, 0.50 mmol), [$PdCl_2(PPh_3)_2$] (30 mg, 0.043 mmol), and CuI (15 mg, 0.079 mmol) in degassed Et_3N (30 ml) was stirred at r.t. for 24 h. (Ethynyl)trimethylsilane was then added, and the mixture was stirred for an additional 8 h. Workup and CC (SiO_2; hexane/CH_2Cl_2 2:1) afforded **8** (55 mg, 19%). R_f 0.6. Yellow-brown solid. M.p. 92–93°. IR (CCl_4): 3092, 2189, 2139, 1605, 1522, 1251. ^{1}H-NMR (200 MHz, $CDCl_3$): 0.21 (*s*, 9 H); 1.09 (*s*, 21 H); 1.10 (*s*, 21 H); 2.98 (*s*, 6 H); 6.58 (*d*, $J = 9.1$, 2 H); 7.34 (*d*, $J = 9.1$, 2 H). ^{13}C-NMR (50.3 MHz, $CDCl_3$): −0.3; 11.2; 11.3; 18.7 (2×); 40.1; 86.3; 100.8; 101.3; 101.6; 103.8; 104.3; 104.4; 109.4; 111.3; 111.5; 115.8; 118.0; 133.2; 150.5. EI-MS (70 eV): 628 (100, M^+). HR-MS: 627.4090 (M^+, $C_{39}H_{61}NSi_3^+$; calc. 627.4112).

1-[4-(Dimethylamino)phenyl]-3-[2-(5-nitro-2-thienyl)ethynyl]-6-(triisopropylsilyl)-4-[2-(triisopropylsilyl)-ethynyl]hex-3-ene-1,5-diyne (**6**). A mixture of **8** (40 mg, 0.064 mmol) and K_2CO_3 (10 mg, 0.07 mmol) in wet MeOH (15 ml) and THF (5 ml) was stirred at r.t. for 2 h. Et_2O and H_2O were added, the org. phase was separated, dried, reduced to 1 ml, and added to Et_3N (15 ml). The soln. was degassed, 2-iodo-5-nitrothiophene (20 mg, 0.078 mmol), [$PdCl_2(PPh_3)_2$] (8 mg, 0.01 mmol), and CuI (4 mg, 0.02 mmol) were added, and the mixture was stirred at r.t. for 12 h. Workup and CC (SiO_2-*H*; hexane/CH_2Cl_2 2:1) afforded **6** (34 mg, 74%). R_f 0.6. Red solid. M.p. 131–132°. UV/VIS ($CHCl_3$): 294 (27200), 341 (21100), 400 (35700), 423 (33900). IR (CCl_4): 2942, 2200, 2178, 2136, 1607, 1337, 1263. ^{1}H-NMR (200 MHz, $CDCl_3$): 1.09 (*s*, 21 H); 1.10 (*s*, 21 H); 2.99 (*s*, 6 H); 6.60 (*d*, $J = 8.9$, 2 H); 7.12 (*d*, $J = 4.4$, 1 H); 7.36 (*d*, $J = 8.9$, 2 H); 7.79 (*d*, $J = 4.4$, 1 H). ^{13}C-NMR

(75 MHz, $CDCl_3$): 11.1 (2×); 18.5 (2×); 40.0; 85.2; 88.2; 95.9; 102.6; 102.7; 103.5; 104.0; 104.1; 108.7; 111.6; 116.5; 116.9; 128.5; 130.4; 131.7; 133.4; 150.8; 151.6. EI-MS (70 eV): 682 (100, M^+). HR-MS: 682.3452 (M^+, $C_{40}H_{54}Si_2N_2O_2S^+$; calc. 682.3444).

1-[4-(Dimethylamino)phenyl]-3-[2-[4-(dimethylamino)phenyl]ethynyl]-4-[2-(5-nitro-2-thienyl)ethynyl]-6-(triisopropylsilyl)hex-3-ene-1,5-diyne (**10**). A mixture of **9** (72 mg, 0.12 mmol) and K_2CO_3 (10 mg, 0.07 mmol) in wet MeOH (20 ml) and THF (5 ml) was stirred at r.t. for 2 h. Et_2O and H_2O were added, the org. phase was separated, dried, reduced to 5 ml, and added to Et_3N (15 ml). The soln. was degassed, 2-iodo-5-nitrothiophene (40 mg, 0.16 mmol), $[PdCl_2(PPh_3)_2]$ (15 mg, 0.021 mmol), and CuI (8 mg, 0.04 mmol) were added, and the mixture was stirred at r.t. for 4 h. Workup and CC (SiO_2-*H*; hexane/CH_2Cl_2 1:1) afforded **10** (34 mg, 45%). R_f 0.4. Black solid. M.p. 158–159°. UV/VIS ($CDCl_3$): 300 (34900), 390 (24100), 477 (34000), 530 (sh, 25200). IR (CCl_4): 2200, 2162, 2136, 1607, 1522, 1322. ^{1}H-NMR (500 MHz, $CDCl_3$): 1.15 (*s*, 3 H); 1.16 (*s*, 18 H); 3.03 (2*s*, 12 H); 6.64 (*d*, *J* = 9.0, 2 H); 6.66 (*d*, *J* = 9.0, 2 H); 7.13 (*d*, *J* = 4.3, 1 H); 7.42 (*d*, *J* = 9.0, 2 H); 7.44 (*d*, *J* = 9.0, 2 H); 7.83 (*d*, *J* = 4.3, 1 H). ^{13}C-NMR (125.8 MHz, $CDCl_3$): 11.4; 18.7; 40.1 (2×); 87.0; 87.1; 88.3; 98.0; 101.5; 102.7; 102.9; 103.0; 108.7; 108.9; 110.3; 111.5; 111.7; 121.8; 128.7; 130.2; 130.8; 131.2; 133.3; 133.5; 150.7; 150.84. EI-MS (70 eV): 647 (0.1, M^+). Anal. calc. for $C_{39}H_{43}N_3O_2SSi$ (645.94): C 72.52, H 6.71, N 6.51; found: C 72.32, H 6.41, N 6.21. X-Ray analysis: see *Fig. 2*.

1-[4-(Dimethylamino)phenyl]-3-[2-[4-(dimethylamino)phenyl]ethynyl]-4-[2-(5-nitro-2-thienyl)ethynyl]-6-(5-nitro-2-thienyl)hex-3-ene-1,5-diyne (**11**). A mixture of **12** (50 mg, 0.085 mmol) and Bu_4NF (0.25 ml, 1M in THF) in wet THF (10 ml) was stirred at r.t. for 1 h. Et_2O and H_2O were added, the org. phase was separated, dried, reduced to 5 ml, and added to Et_3N (15 ml). The soln. was degassed, 2-iodo-5-nitrothiophene (50 mg, 0.19 mmol), $[PdCl_2(PPh_3)_2]$ (8 mg, 0.01 mmol), and CuI (4 mg, 0.03 mmol) were added, and the mixture was stirred at r.t. for 16 h. Workup and CC (SiO_2-*H*; hexane/CH_2Cl_2 1:5) afforded **12** (27 mg, 52%). R_f 0.6. Black solid. M.p. >270° (dec.) UV/VIS ($CHCl_3$): 297 (39800), 377 (30500), 498 (48400), 570 (sh, 33600). IR (CCl_4): 2150, 1600, 1522, 1317. ^{1}H-NMR (500 MHz, $CDCl_3$): 3.06 (*s*, 12 H); 6.67 (*d*, *J* = 9.0, 4 H); 7.20 (*d*, *J* = 4.3, 2 H); 7.47 (*d*, *J* = 9.0, 4 H); 7.85 (*d*, *J* = 4.3, 2 H). ^{13}C-NMR (75 MHz, $Cl_2DCCDCl_2$): 40.4; 88.1; 89.8; 96.5; 105.9; 107.7; 107.9; 112.0; 124.1; 129.4; 131.0; 131.6; 134.0; 151.2; 151.4. FAB-MS: 616 (100, M^+). X-Ray analysis: see *Fig. 3*.

1-[4-(Dimethylamino)phenyl]-3-[2-[4-(dimethylamino)phenyl]ethynyl]-4-[2-(4-nitrophenyl)ethynyl]-6-(5-nitro-2-thienyl)]hex-3-ene-1,5-diyne (**13**). A mixture of **14** (34 mg, 0.053 mmol) and Bu_4NF (0.1 ml, 1M in THF) in wet THF (10 ml) was stirred at r.t. for 1 h. Et_2O and H_2O were added, the org. phase was separated, dried, reduced to 5 ml, and added to Et_3N (15 ml). The soln. was degassed, 2-iodo-5-nitrothiophene (20 mg, 0.078 mmol), $[PdCl_2(PPh_3)_2]$ (8 mg, 0.01 mmol), and CuI (4 mg, 0.03 mmol) were added, and the mixture was stirred at r.t. for 4 h. Workup and CC (SiO_2-*H*; hexane/CH_2Cl_2 1:5) afforded **13** (21 mg, 66%). R_f 0.6. Black solid. M.p. 210° (dec). UV/VIS ($CHCl_3$): 296 (40700), 356 (27700), 484 (42000), 544 (sh, 33300). IR (CCl_4): 3091, 2922, 2144, 1600, 1521, 1311. ^{1}H-NMR (300 MHz, $CDCl_3$): 3.03 (*s*, 12 H); 6.63 (*d*, *J* = 9.0, 2 H); 6.63 (*d*, *J* = 8.7, 2 H); 7.17 (*d*, *J* = 4.2, 1 H); 7.41 (*d*, *J* = 8.7, 2 H); 7.44 (*d*, *J* = 9.0, 2 H); 7.67 (*d*, *J* = 8.7, 2 H); 7.82 (*d*, *J* = 4.2, 1 H); 8.20 (*d*, *J* = 8.7, 2 H). ^{13}C-NMR (75 MHz, $CDCl_3$) (some peaks not observed): 40.0 (2×); 87.5; 87.6; 89.1; 92.3; 95.9; 96.7; 104.6; 108.2; 108.3; 108.6; 111.7 (2×); 123.5; 123.8; 128.9; 129.9; 130.8; 131.1; 133.5; 133.6; 147.2; 151.1; 151.2. FAB-MS: 610 (100, M^+). X-Ray analysis: see *Fig. 4*.

*1-[3,5-Di(*tert*-butyl)phenyl]-3-[2-[3,5-di(*tert*-butyl)phenyl]ethynyl]-4-[2-(2-thienyl)ethynyl]-6-(2-thienyl)-hex-3-ene-1,5-diyne* (**15**). A mixture of **16** (0.20 g, 0.31 mmol) and K_2CO_3 (10 mg, 0.07 mmol) in wet MeOH (20 ml) and THF (5 ml) was stirred at r.t. for 2 h. Et_2O and H_2O were added, the org. phase was separated, dried, reduced to 5 ml, and added to Et_3N (30 ml). The soln. was degassed, 2-iodothiophene (0.143 g, 0.68 mmol), $[PdCl_2(PPh_3)_2]$ (20 mg, 0.03 mmol), and CuI (10 mg, 0.06 mmol) were added, and the mixture was stirred at r.t. for 48 h. Workup and CC (SiO_2-*H*; hexane/CH_2Cl_2 4:1) afforded **16** (31 mg, 15%). R_f 0.3. Orange solid. M.p. 178–180° (dec.). UV/VIS ($CHCl_3$): 310 (31800), 334 (23800), 376 (18700), 433 (29300). IR (CCl_4): 3106, 3074, 2964, 2211, 2183, 1583, 1478, 1361. ^{1}H-NMR (200 MHz, $CDCl_3$): 1.31 (br. *s*, 36 H); 7.01 (*dd*, *J* = 3.4, 4.4, 2 H); 7.34 (*d*, *J* = 4.4, 2 H); 7.38 (*d*, *J* = 3.4, 2 H); 7.43 (br. *s*, 2 H); 7.45 (br. *s*, 4 H). ^{13}C-NMR (75 MHz, $CDCl_3$): 31.2; 34.8; 86.4; 91.1; 92.1; 100.9; 115.8; 117.5; 121.6; 122.7; 123.8; 126.4; 127.4; 128.6; 133.0; 151.0. EI-MS: 664 (100, M^+). HR-MS 664.3209 (M^+, $C_{46}H_{48}S_2^+$; calc. 664.3197).

REFERENCES

[1] 'Conjugated Polymers and Related Materials', Eds. W. R. Salaneck, I. Lundström, B. Rånby, Oxford University Press, Oxford, 1993.

[2] Y. Rubin, C. B. Knobler, F. Diederich, *Angew. Chem.* **1991**, *103*, 708; *Angew. Chem., Int. Ed.* **1991**, *30*, 698.

[3] J. Anthony, A. M. Boldi, Y. Rubin, M. Hobi, V. Gramlich, C. B. Knobler, P. Seiler, F. Diederich, *Helv. Chim. Acta* **1995**, *78*, 13.
[4] R. R. Tykwinski, F. Diederich, *Liebigs Ann./Recueil* **1997**, 649.
[5] R. R. Tykwinski, M. Schreiber, R. Pérez Carlón, F. Diederich, V. Gramlich, *Helv. Chim. Acta* **1996**, *79*, 2249.
[6] R. R. Tykwinski, M. Schreiber, V. Gramlich, P. Seiler, F. Diederich, *Adv. Mater.* **1996**, *8*, 226.
[7] A. Hilger, J.-P. Gisselbrecht, R. R. Tykwinski, C. Boudon, M. Schreiber, R. E. Martin, H. P. Lüthi, M. Gross, F. Diederich, *J. Am. Chem. Soc.* **1997**, *119*, 2069.
[8] C. Bosshard, R. Spreiter, P. Günter, R. R. Tykwinski, M. Schreiber, F. Diederich, *Adv. Mater.* **1996**, *8*, 231.
[9] R. Spreiter, C. Bosshard, G. Knöpfle, P. Günter, R. R. Tykwinski, M. Schreiber, F. Diederich, *J. Phys. Chem. B* **1998**, *102*, 29.
[10] M. Schreiber, R. R. Tykwinski, F. Diederich, R. Spreiter, U. Gubler, C. Bosshard, I. Poberaj, P. Günter, C. Boudon, J.-P. Gisselbrecht, M. Gross, U. Jonas, H. Ringsdorf, *Adv. Mater.* **1997**, *9*, 339.
[11] U. Gubler, R. Spreiter, C. Bosshard, P. Günter, R. R. Tykwinski, F. Diederich, *Appl. Phys. Lett.* **1998**, *73*, 2396.
[12] R. E. Martin, U. Gubler, C. Boudon, V. Gramlich, C. Bosshard, J.-P. Gisselbrecht, P. Günter, M. Gross, F. Diederich, *Chem. Eur. J.* **1997**, *3*, 1505.
[13] R. R. Tykwinski, U. Gubler, R. E. Martin, F. Diederich, C. Bosshard, P. Günter, *J. Phys. Chem. B* **1998**, *102*, 4451.
[14] P. R. Varanasi, A. K.-Y. Jen, J. Chandrasekhar, I. N. N. Namboothiri, A. Rathna, *J. Am. Chem. Soc.* **1996**, *118*, 12443.
[15] a) I. D. L. Albert, T. J. Marks, M. A. Ratner, *J. Am. Chem. Soc.* **1997**, *119*, 6575; b) I. D. L. Albert, J. O. Morley, D. Pugh, *J. Phys. Chem.* **1995**, *99*, 8024.
[16] V. Keshari, W. M. V. K. Wijekoon, P. N. Prasad, S. P. Karna, *J. Phys. Chem.* **1995**, *99*, 9045; S. P. Karna, Y. Zhang, M. Samoc, P. N. Prasad, B. A. Reinhardt, A. G. Dillard, *J. Chem. Phys.* **1993**, *99*, 9984.
[17] C. Adant, J.-L. Brédas, M. Dupuis, *J. Phys. Chem. A* **1997**, *101*, 3025.
[18] C. Cai, I. Liakatas, M.-S. Wong, M. Bösch, C. Bosshard, P. Günter, S. Concilio, N. Tirelli, U. W. Suter, *Org. Lett.* **1999**, *1*, 1847; F. Steybe, F. Effenberger, U. Gubler, C. Bosshard, P. Günter, *Tetrahedron* **1998**, *54*, 8469; F. Pan, C. Bosshard, M. S. Wong, C. Serbutoviez, K. Schenk, V. Gramlich, P. Günter, *Chem. Mater.* **1997**, *9*, 1328.
[19] Y.-K. Wang, C.-F. Shu, E. M. Breitung, R. J. McMahon, *J. Mater. Chem.* **1999**, *9*, 1449.
[20] S. Thayumanavan, J. Mendez, S. R. Marder, *J. Org. Chem.* **1999**, *64*, 4289.
[21] M. G. Hutchins, I. Ferguson, D. J. McGeein, J. O. Morley, J. Zyss, I. Ledoux, *J. Chem. Soc., Perkin Trans. 2* **1995**, 171.
[22] P. Boldt, G. Bourhill, C. Bräuchle, Y. Jim, R. Kammler, C. Müller, J. Rase, J. Wichern, *Chem. Commun.* **1996**, 793.
[23] S.-S. P. Chou, G.-T. Hsu, H.-C. Lin, *Tetrahedron Lett.* **1999**, *40*, 2157; S.-S. P. Chou, D.-J. Sun, H.-C. Lin, P.-K. Yang, *Chem. Commun.* **1996**, 1045.
[24] A. K.-Y. Jen, Y. Cai, P. V. Bedworth, S. R. Marder, *Adv. Mater.* **1997**, *9*, 132; V. P. Rao, A. K.-Y. Jen, Y. M. Cai, *Chem. Commun.* **1996**, 1237; K. Y. Wong, A. K.-Y. Jen, V. P. Rao, K. J. Drost, *J. Chem. Phys.* **1994**, *100*, 6818; V. P. Rao, K. Y. Wong, A. K.-Y. Jen, K. J. Drost, *Chem. Mater.* **1994**, *6*, 2210; K. Y. Wong, A. K.-Y. Jen, V. P. Rao, *Phys. Rev. A* **1994**, *49*, 3077; V. P. Rao, A. K.-Y. Jen, K. Y. Wong, K. J. Drost, *J. Chem. Soc., Chem. Commun.* **1993**, 1118.
[25] F. Chérioux, H. Maillotte, P. Audebert, J. Zyss, *Chem. Commun.* **1999**, 2083.
[26] C. Moreau, F. Serein-Spirau, J.-F. Létard, R. Lapouyade, G. Jonusauskas, C. Rullière, *J. Phys. Chem. B* **1998**, *102*, 1487.
[27] K. Kamada, M. Ueda, T. Sakaguchi, K. Ohta, T. Fukumi, *J. Opt. Soc. Am. B* **1998**, *15*, 838.
[28] T. Yamamoto, Z.-H. Zhou, T. Kanbara, M. Shimura, K. Kizu, T. Maruyama, Y. Nakamura, T. Fukuda, B.-L. Lee, N. Ooba, S. Tomaru, T. Kurihara, T. Kaino, K. Kubota, S. Sasaki, *J. Am. Chem. Soc.* **1996**, *118*, 10389.
[29] L.-T. Cheng, W. Tam, S. R. Marder, A. E. Stiegman, G. Rikken, C. W. Spangler, *J. Phys. Chem.* **1991**, *95*, 10643.
[30] M.-T. Zhao, B. P. Singh, P. N. Prasad, *J. Chem. Phys.* **1988**, *89*, 5535.
[31] S. Takahashi, Y. Kuroyama, K. Sonogashira, N. Hagihara, *Synthesis* **1980**, 627; K. Sonogashira, in 'Metal-catalyzed Cross-coupling Reactions', Eds. F. Diederich, P. J. Stang, Wiley-VCH, Weinheim, 1998, pp. 203–229.
[32] H. Kreis, *Ber.* **1884**, *17*, 2073.
[33] R. E. Martin, J. Bartek, F. Diederich, R. R. Tykwinski, E. Meister, A. Hilger, H. P. Lüthi, *J. Chem. Soc., Perkin Trans. 2* **1998**, 233.

[34] J. Anthony, A. M. Boldi, C. Boudon, J.-P. Gisselbrecht, M. Gross, P. Seiler, C. B. Knobler, F. Diederich, *Helv. Chim. Acta* **1995**, *78*, 797.
[35] D. J. Dawson, J. D. Frazier, P. J. Brock, R. J. Twieg, 'Polymers for High Technology', ACS Symp. Ser. Vol. 346, ACS, Washington, D.C. 1987, pp. 445–456.
[36] R. Faust, F. Diederich, V. Gramlich, P. Seiler, *Chem. Eur. J.* **1995**, *1*, 111.
[37] C. Dehu, F. Meyers, J.-L. Brédas, *J. Am. Chem. Soc.* **1993**, *115*, 6198.
[38] J. L. Brédas, F. Meyers, *Nonlinear Opt.* **1991**, *1*, 119.
[39] A. E. Stiegman, E. Graham, K. J. Perry, L. R. Khundkar, L.-T. Cheng, J. W. Perry, *J. Am. Chem. Soc.* **1991**, *113*, 7658.
[40] A. E. Stiegman, V. M. Miskowski, J. W. Perry, D. R. Coulter, *J. Am. Chem. Soc.* **1987**, *109*, 5884.
[41] E. M. Graham, V. M. Miskowski, J. W. Perry, D. R. Coulter, A. E. Stiegman, W. P. Schaefer, R. E. Marsh, *J. Am. Chem. Soc.* **1989**, *111*, 8771.
[42] C. Bosshard, G. Knöpfle, P. Prêtre, P. Günter, *J. Appl. Phys.* **1992**, *71*, 1594.
[43] J. Stradins, R. Gavars, L. Baumane, *Electrochimica Acta* **1983**, *28*, 495.
[44] M. C. Zerner, ZINDO Quantum Chemical Program Package, University of Gainsville, FL, 1997.
[45] M. J. Frisch, G. W. Trucks, H. B. Schlegel, P. M. W. Gill, B. G. Johnson, M. A. Robb, J. R. Cheeseman, T. A. Keith, G. A. Petersson, J. A. Montgomery, K. Raghavachari, M. A. Al-Laham, V. G. Zakrzewski, J. V. Ortiz, J. B. Foresman, J. Cioslowski, B. B. Stefanov, A. Nanayakkara, M. Challacombe, C. Y. Peng, P. Y. Ayala, W. Chen, M. W. Wong, J. L. Andres, E. S. Replogle, R. Gomperts, R. L. Martin, D. J. Fox, J. S. Binkley, D. J. Defrees, J. Baker, J. J. P. Stewart, M. Head-Gordon, C. Gonzalez, J. A. Pople, Gaussian 94, (Revision C.3), *Gaussian*, *Inc.*, Pittsburgh, PA, 1995.
[46] J. P. P. Stewart, MOPAC: A General Molecular Orbital Package, V. 6.0, Quantum Chemistry Program Exchange (QCPE), 1990.
[47] P. F. Flükiger, MOLEKEL V. 2.6, University of Geneva and CSCS Manno, Switzerland, 1997.
[48] J. Cornil, D. Beljonne, J.-L. Brédas, *J. Chem. Phys.* **1995**, *103*, 834; J. Cornil, D. Beljonne, J.-L. Brédas, *J. Chem. Phys.* **1995**, *103*, 842.
[49] D. Philp, V. Gramlich, P. Seiler, F. Diederich, *J. Chem. Soc., Perkin Trans. 2* **1995**, 875.

Received April 13, 2000